



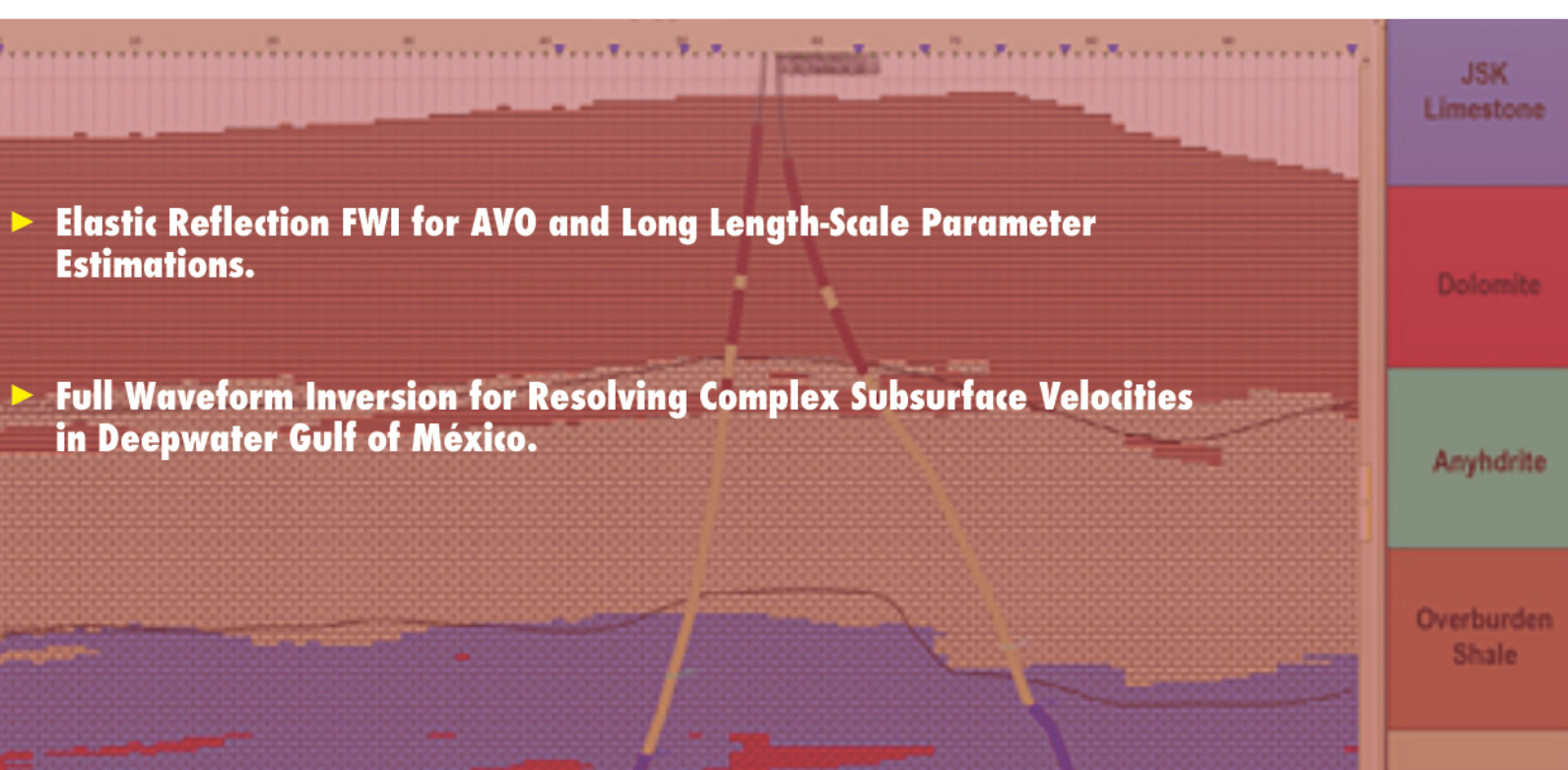
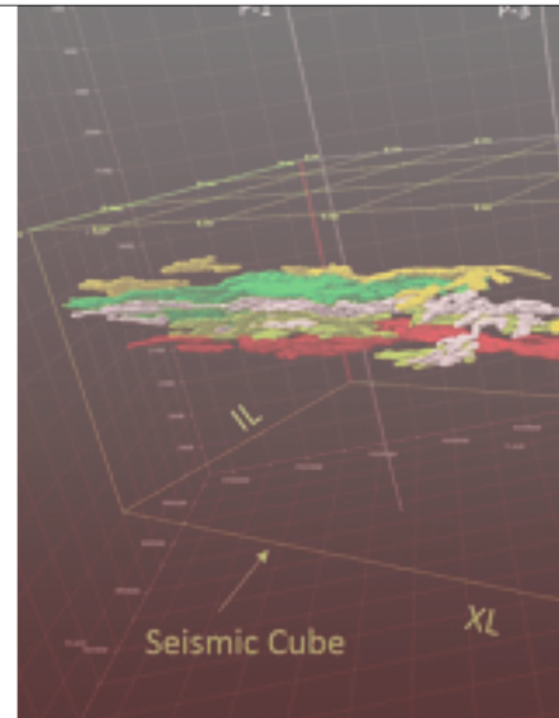
Asociación Mexicana de Geofísicos
de Exploración, A.C.

Segunda Generación

Volumen 2 | Número 1 | Enero-Marzo 2019

Inversión Sísmica

- Identifying Brittle Zones for Natural Gas Condensate Heterogeneous Reservoirs Using Rock Physics and Seismic Inversion.
- Geo-predicción: Inversión Simultánea en Impedancia y Facies Sísmicas Para Caracterizar Contenido de Roca/Fluido en Yacimientos de Carbonatos.





Asociación Mexicana de Geofísicos de Exploración, A.C.

COMITÉ EJECUTIVO AMGE 2018-2020

Jorge Barrios Rivera

Presidente

Gerardo Clemente Martínez
Vicepresidente

Otila Mayes Mellado
Pro-Secretaria

Eduardo T. Ramírez Reséndiz
Pro-Tesorero

Efraín Méndez Hernández
Editorial

Humberto Samuel Arévalo López
Editorial

Sergio Chávez Pérez
Relaciones Internacionales

Nora Alejandra Rodríguez González
Comunicación y Redes Sociales

Dámaso Contreras Tebar
Secretario

Rosa Irene Ríos Cedeño
Tesorera

Humberto Salazar Soto
Coordinación Eventos Técnicos

Raúl Del Valle García
Editorial

Claudia Beristain Suárez
Coordinación de Membresía

Francisco Rubén Rocha De La Vega
Capítulos Estudiantiles

Patricia Oceguera Serrano
Coordinación de Jubilados

Presidentes Delegacionales:

Rubén Darío Martínez Macías, Houston; Juan Carlos Salguero Arguelles, Reynosa; Juan Maldonado Lezama, Tampico; Arturo Bautista López, Poza Rica; Gabriel González Covarrubias, Veracruz; Juan Manuel Nájera García, Villahermosa; José Alberto Santana Fernández, Carmen; Francisco Rubén Rocha De La Vega, CDMX.

Para someter manuscritos en el Boletín Técnico AMGE – Segunda Generación, así como conocer las normas editoriales y guía de publicación, favor de comunicarse con alguno de los siguientes editores:



Raúl del Valle García
Email: rvalleg@imp.mx



Efraín Méndez Hernández
Email: emendez2310@gmail.com

DERECHOS DE AUTOR

Boletín Técnico de la AMGE, Segunda Generación, es publicado cuatro veces al año por la Asociación Mexicana de Geofísicos de Exploración, A.C., Campo Tamulte 117, Col. Carrizal, Villahermosa Centro, Tabasco, C.P. 86038. El título del Boletín, así como el contenido se encuentran debidamente autorizados y protegidos. Publicada trimestralmente por la Asociación Mexicana de Geofísicos de Exploración, A.C., Volumen 2, Número 1, Enero-Marzo 2019.

SOBRE ARTÍCULOS

Los artículos del nuevo Boletín Técnico AMGE, en su Segunda Generación, son presentados a nuestros socios bajo el respaldo de textos técnicos que han sido dados a conocer en el Congreso Mexicano del Petróleo, de manera anual, y que poseen tanto un formato establecido como autorizaciones requeridas, y han sido ya arbitreados por expertos en la materia.

Esta edición reproduce fielmente las imágenes de origen y el contenido de los autores.

COLABORADORES

- **Director:** Carlos Pozos
- **Editores:** Francisco Abad, Rebeca Sánchez
- **Diseño:** Pepe Tepezano
pozos_sotocarlos@yahoo.com.mx



Editorial

Este boletín se concentra en temas de inversión sísmica y sus aplicaciones. Cabe mencionar que hay dos técnicas predominantes referentes a inversión sísmica. La primera, conocida como inversión de impedancia, no es una inversión geofísica rigurosa ya que parte de un modelo convolucional. No obstante, es la inversión más utilizada en la industria por razones prácticas y económicas, siendo de fácil implementación y aplicada con relativo éxito a muchos problemas de la industria petrolera. La otra inversión, mucho más rigurosa, es la inversión de forma de onda completa ('Full Waveform Inversion', FWI). Esta inversión, de cómputo desafiantes, comprende técnicas de imagen sísmica de alta resolución basada en el uso del contenido total de las trazas sísmicas, con el objetivo de extraer parámetros físicos (velocidad y densidad) del medio donde se propagaron las ondas. El primer ingrediente importante en la FWI es un eficiente algoritmo del modelo directo, que es requerido para estimar eficientemente el gradiente y el Hessiano que son parte del proceso de inversión sísmica. La optimización local no garantiza en la mayoría de los casos prácticos una convergencia adecuada debido a la precisión limitada del modelo inicial, la falta de bajas frecuencias y la presencia de ruido. Estudios recientes indican que las frecuencias bajas y 'offsets' de apertura amplia pueden ser un ingrediente clave para construir exitosamente los modelos de velocidad utilizando FWI. Aún con la adquisición multicomponente de gran apertura y de acimut, sólo es viable la FWI acústica 3D. De manera estricta, el modelo directo debería ser por lo menos elástico y de manera óptima debería contener anisotropía, viscoelasticidad o poroelasticidad. A la fecha esto no es ni tecnológica, ni económicamente factible. Por ejemplo, el método de diferencias finitas que se usa comúnmente para el campo de onda, se ve fuertemente afectado por la dispersión numérica a medida que aumenta el ancho de banda de frecuencia, lo que nos obliga a usar retículas más finas, lo que posteriormente aumenta el costo computacional. El costo se vuelve prohibitivamente alto para ondas en medios anisótropos y elásticos debido a las variaciones espaciales de velocidad. Por esta razón, el FWI de alta resolución sigue siendo un desafío que limita la aplicabilidad potencial. Se ha calculado que pasar del modelo directo acústico (escalar) al modelo elástico (vectorial), aumenta 2 órdenes de magnitud el costo de cómputo.

El primer trabajo presenta un estudio para la estimación de fragilidad a través de un análisis integral de las propiedades elásticas provenientes de la inversión de impedancia y del modelado de física de rocas, apoyándose de información de registro de pozo.

El segundo trabajo implementa la inversión simultánea de impedancia y facies sísmicas en un campo con formaciones dolomitizadas. De acuerdo con este trabajo, el método utilizado de inversión sísmica, considera elementos categóricos (facies) y continuos (impedancia en función de las facies), dando como resultado una caracterización litológica.

El siguiente trabajo es un esfuerzo teórico-numérico para realizar la inversión de onda completa en un medio elástico ortorrómbico. Se demuestra su efectividad práctica en la inversión simultánea para presión y velocidad de corte de modelos sintéticos propuestos.

El último artículo en este boletín presenta la inversión de forma de onda completa aplicado en aguas profundas del Golfo de México. Se presenta mejor resolución del subsuelo al utilizar datos con acimut de apertura amplia.

COMITÉ EDITORIAL 2018-2020

Raúl del Valle García
Efraín Méndez Hernández





Contenido

Tema: Inversión Sísmica

Identifying Brittle Zones for Natural Gas Condensate Heterogeneous Reservoirs Using Rock Physics and Seismic Inversion

Mario Di Luca Vingelli* (Frontera Energy Corp.); Trino Salinas (Independent Advisor); Roderick Pérez (Independent Advisor)

8

Geo-Predicción: Inversión Simultánea En Impedancia y Facies Sísmicas para Caracterizar Contenido de Roca/Fluido en Yacimientos de Carbonatos

Dante Granados, Alejandro Salas (PEMEX), Adrien Caudron, Marco Vázquez (APOGEE), Alan Mur, Gabriela D'Aubeterre, Simón Payne (IKON)

22

Elastic Reflection FWI for AVO and Long Length-Scale Parameter Estimations

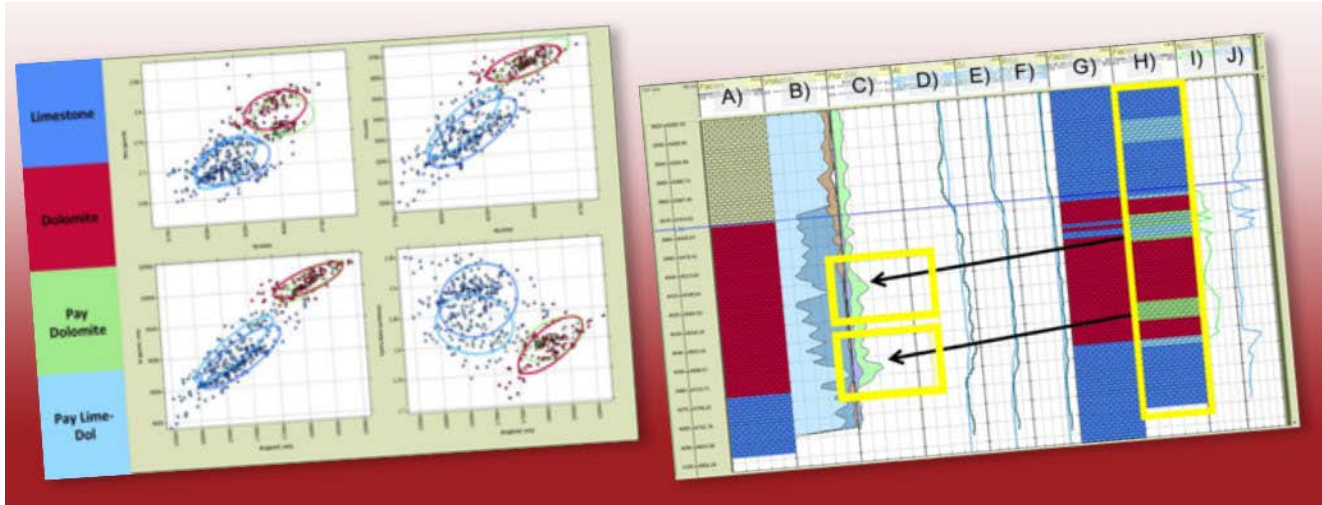
Peng Shen (Chevron Energy Technology Company), Uwe Albertin (Chevron Energy Technology Company), and Anusha Sekar (Chevron Energy Technology Company)

28

Full Waveform Inversion for Resolving Complex Subsurface Velocities in Deepwater Gulf of México

Bin Yu (CGG), Ravi Kumar (CGG), Brad Wray (CGG), Katarina Jonke (CGG), Heiner Sarmiento (CGG)

34



Identifying Brittle Zones for Natural Gas Condensate Heterogeneous Reservoirs Using Rock Physics and Seismic Inversion

Mario Di Luca Vingelli (Frontera Energy Corp.); Trino Salinas (Independent Advisor); Roderick Pérez (Independent Advisor)

CMP2018_GC56
Artículo presentado
en el CMP / 2018

● Abstract

The purpose of this study is to identify brittle zones in a heterogeneous reservoir through the estimation and analysis of elastic properties resulting from seismic inversion.

The target is a natural gas condensate reservoir, composed of sandstone sheets interbedded with shale, with poor lateral continuity and low permeability (nano-millidarcy). The vertical resolution in the logs is not enough to resolve sandstones sheets. Given that the laminated sandstones grouped in multiple cycles and are embedded in a thick shale section, it is possible to differentiate this lithological arrangement, using the seismic and well log data.

The reservoir is characterized by low permeability and poor connectivity, hydraulic fracturing stimulation is needed to produce it, so the brittleness estimation is necessary for the reservoir characterization.

These reservoir properties lead to developing a specialized geophysical analysis to determine the mineralogical based brittleness index, and correlation to the well logs elastic parameters.

Rock physics analysis performed in the key wells lead to a quantitative interpretation of seismic inversion results that allowed mapping geobodies for five layers inside target interval as final output, those represent the reservoir in the area prone to requiring stimulation by hydraulic fracturing.

Introduction

The study area is located in the Lower Magdalena Valley Basin, the target interval (approximately 2000 ft in thickness–Age Miocene) is informally defined as FP-H3 of the Porquero Formation, which depositional environment correspond to deep water deposits

(submarine fans), transported by turbiditic currents. (Reyes Harker et al., 2000 & Ghosh et al., 2013).

This paper demonstrates that rock physics and pre-stack seismic inversion parameters, integrated with geological and well log data, allow to characterize the FP-H3 interval in the Porquero Formation for the studied area.

In the study area, the reservoir requires hydraulic fracturing stimulation for production. To distinguish the areas to be stimulated we used the brittleness calculation from elastic properties: Poisson Ratio (σ) and Young's Modulus (E).

The conventional core information, petrophysical evaluation and mineralogical logs with the calculated rock brittleness and Lambda-Rho ($\lambda\rho$) vs. Mu-Rho ($\mu\rho$) crossplots, were used to define the trending zones in Lambda-Rho ($\lambda\rho$) vs Mu-Rho ($\mu\rho$) graphs, relating to the rock quality and present fluids in the FP-H3 interval.

Figure 1, shows the well location and seismic data available used for this study. Vp, Vs and density logs were available from P-2, P-3, P-4 and P-5 wells.

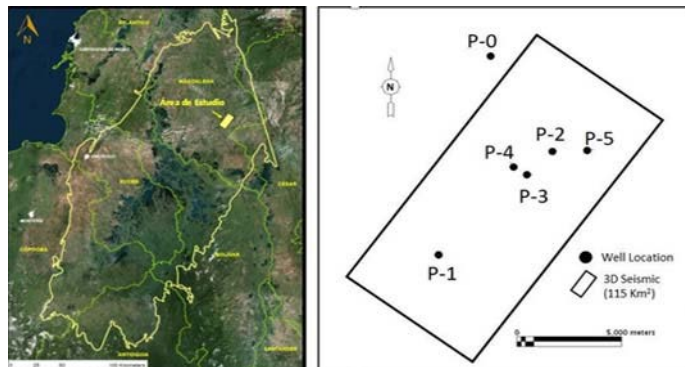


Figure 1. Study area location.

Quantitative Interpretation

Rock Physics Analysis

Figure 2 shows the well log response in the FP-H3 interval, for P-2 well. Which is a main shaly section with sandstone beds that range from a few inches to 1 ft, these properties are confirmed in cores and image logs (Figure 3).

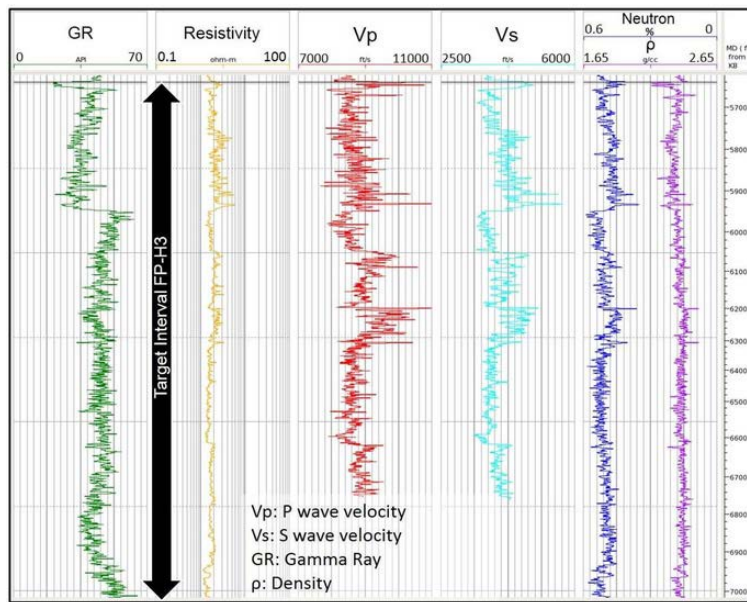


Figure 2. Well logs for P-2 well in the target interval.

Although the logs show high clay content and low HC saturation, Vp and ρ logs correlate to higher resistivities suggestive of gas presence.

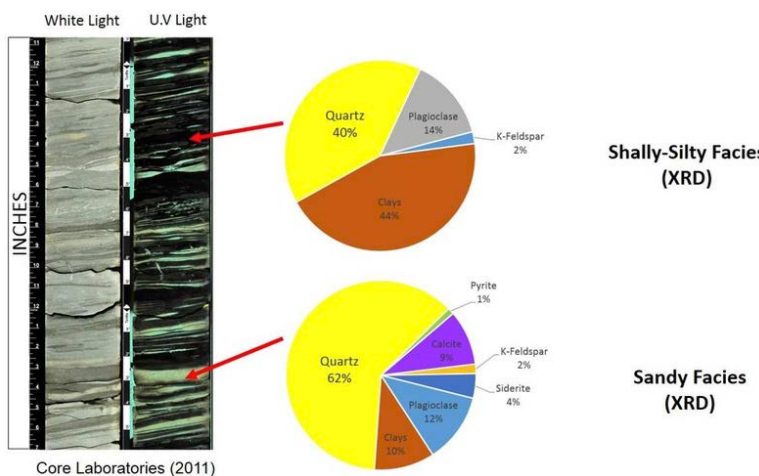


Figure 3. P-2 core and X-Ray diffraction (XRD) in shales and sandstones. Corelab (2010).

In FP-H3 interval, there is no overlap between Neutron and Density logs for gas reservoirs. Gas production was obtained after hydraulic fracturing intervals of less than 5 ft in thickness which shows the higher resistivities intervals (3.8 - 5.9 ohm-m).

The reservoir conditions lead to an attenuated gas response in the logs (Betancourt, 2015), and must be considered during the rock physics analysis for an accurate reservoir characterization.

The reservoir petrophysical behavior was analyzed in detail, by use of several crossplots among different elastic properties. The purpose was to determine the importance and power of these properties to discriminate different lithologies and fluids in the area. The result of this analysis lead to define the LMR ($\lambda\rho$ and $\mu\rho$) crossplots as the best discriminator.

Lamé's incompressibility parameter λ relates uniaxial and lateral strain to uniaxial stress. The λ is primarily a longitudinal measure and hence "orthogonal" to Lamé's rigidity parameter μ a quantity that relates shearing stress to strain. Dipole sonic coupled with P-wave sonic and density logs provide a direct measure of Lamé parameters λ and μ at the well (Goodway, 2007).

Compressional and shear velocities V_p and V_s can be written in terms of Lamé's parameters λ and μ and bulk density ρ :

$$V_p = \sqrt{(\lambda + 2\mu)/\rho} \quad (1)$$

$$and \quad V_s^2 = (\mu/\rho) \quad (2)$$

Seismic reflections are sensitive to changes in P- and S-impedances, Z_p and Z_s . We can therefore estimate Lamé impedances (moduli-density relationships) from surface seismic data as follows:

$$\mu\rho = (\rho V_s)^2 = Z_s^2 \quad (3)$$

$$and \quad \lambda\rho = (\rho V_p)^2 - 2(\rho V_s)^2 = Z_p^2 - 2Z_s^2 \quad (4)$$

Figure 4 shows Lambda-Rho ($\lambda\rho$) vs. Mu-Rho ($\mu\rho$) crossplots for the target interval in wells P-4 and P-5.

High porosities correspond to $\lambda\rho$ and $\mu\rho$ low values (Figure 4-c), thus Lamé Impedance parameters ($\lambda\rho$ and $\mu\rho$ or LMR) allow having a good discrimination for porosity in the target interval. One indicator of low porosity in sand's facies is high density. The 4-d plot shows how the samples with the lower permeabilities (higher density values), correspond to high $\lambda\rho$ and $\mu\rho$ values. In the 4-a and 4-b crossplots we observe an evident samples separation according to lithology and fluid saturation.

P-4 and P-5 are the only wells with mineralogical logs, those were used to obtain the quartz volume (V_q). Using V_q in crossplots $\lambda\rho$ versus $\mu\rho$ analysis (Figure 5) gives a clear trend for the samples discrimination as a function of quartz content for both parameters of Lamé Impedance.

When comparing the shale region (Figure 4-a) with the obtained results in Figure 5, it is noted that some of the shale samples from Porquero Formation has a high quartz content. This is confirmed by the X Ray Diffraction (XRD) results performed in P-2 well samples (Figure 3).

After analyzing crossplots Lambda-Rho ($\lambda\rho$) versus Mu-Rho ($\mu\rho$), together with the well petrophysical information (V_{sh} and S_w), it

was possible to discriminate sand and shale (Figure 4-a and 4-b). A shale discrimination as a function of its quartz content was also obtained (Figure 5).

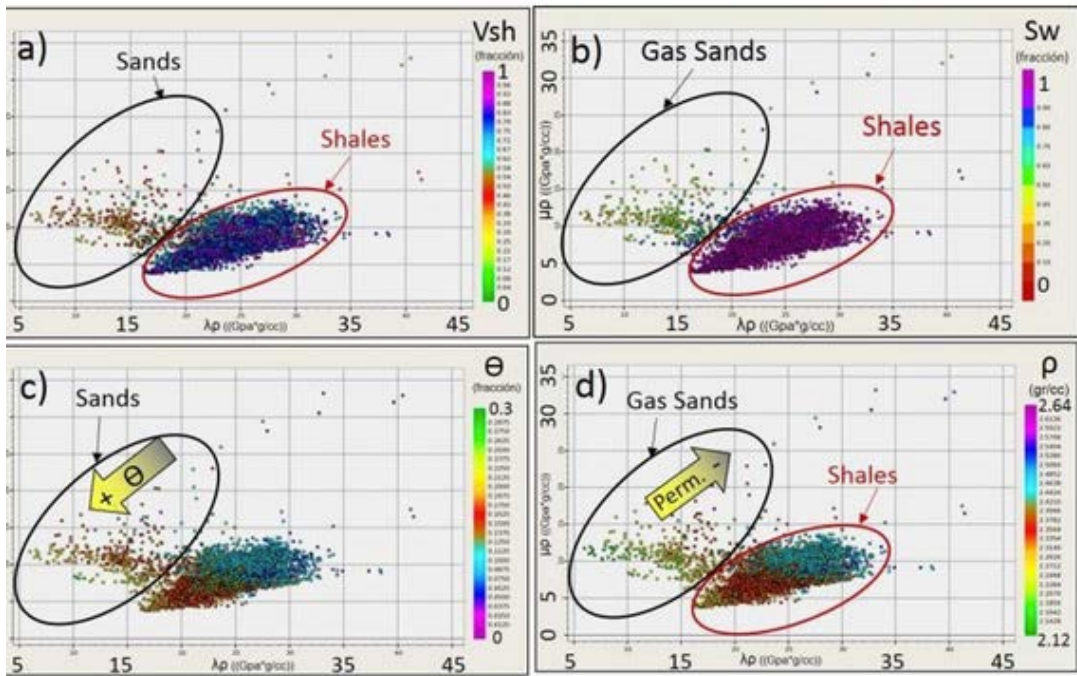


Figure 4. Crossplots $\lambda\rho$ versus $\mu\rho$, FP-H3 interval, wells P-4 and P-5. Colored samples a) V_{sh} , b) Sw , c) θ and d) ρ .

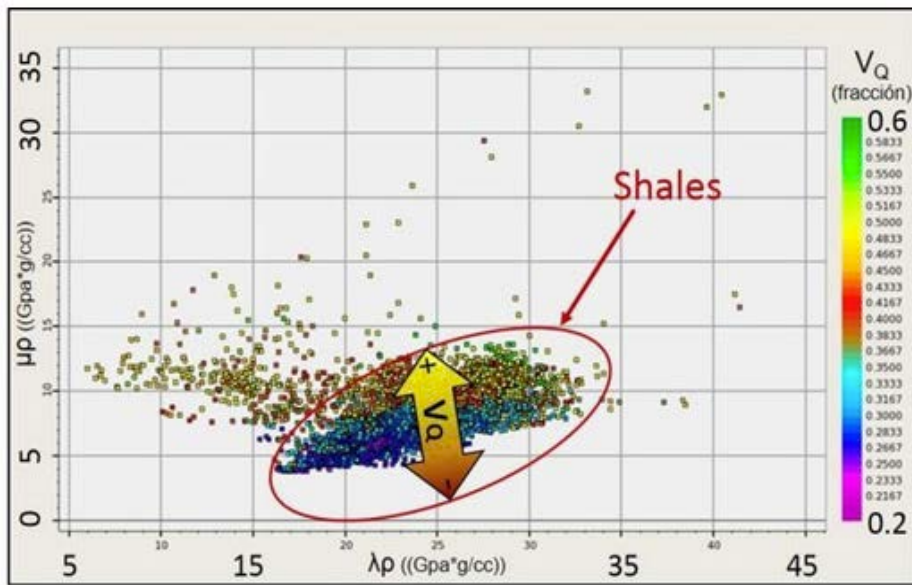


Figure 5. Crossplot $\lambda\rho$ versus $\mu\rho$, FP-H3 interval, P-4 and P-5 wells. V_Q colored samples. Several researchers have proposed brittleness definitions based on mineral content logs for reservoir characterization (Bo Zhang et al., 2015); Herwanger et al. (2015) explain that according the mineralogical definition, brittleness is a measure of the volume fraction of stiff mineral (such as quartz) as part of the entire matrix volume. The results shown in Figure 5 suggest a correlation between rock quartz volume, brittleness and the LMR parameters in this study.

From previous investigations about reservoir characterization, there are three methodologies to estimate brittleness of rocks: 1) Use of elastic properties, 2) Mineralogical content and, 3) Using rock resistance measures obtained in the lab (Herwanger et al., 2015). In this study we used the first two, given that there is not available lab data.

Brittleness calculation

- Using elastic properties we determined Average Brittleness, this is dependent on the Poisson Ratio (σ) and Young's Modulus (E) (Equation (5)) Grieser and Bray (2007).

$$BRI_avg \text{ (%)} = \frac{100}{2} * \left(\frac{\sigma_{max} - \sigma}{\sigma_{max} - \sigma_{min}} + \frac{E - E_{min}}{E_{max} - E_{min}} \right) \quad (5)$$

- To perform the Brittleness estimation from mineralogical data (Brittleness Index) Jarvie et al. (2007), Equation was used (Equation 6). This calculation was completed only in the wells P-4 and P-5, which have mineralogical logs.

$$BRI_I = (V_Q / (V_Q + V_{cal} + V_{arc})) \quad (6)$$

Figure 6 shows P-5 well logs. In the last track to the right are the results of:

- In red, Average Brittleness (BRI_avg) using the Grieser and Bray (2007) Equation and,
- In blue, Brittleness estimation using Jarvie et al. (2007) to get the Brittleness Index (BRI_I).

Both methodologies, Brittleness Average and Brittleness Index do not coincide in value as shown in Figure 6. The difference in magnitudes of Brittleness values are due to:

1. Average Brittleness considers in its equation maximum and minimum values for the Poisson ratio (σ) and Young's Modulus (E), unlike the Brittleness Index is based on mineralogical logs.
2. Another reason for the difference between both Brittleness estimations is that the mineralogical log is a measure of the rock matrix and does not consider the pore rock fluids. On the other hand the elastic properties: Poisson ratio (σ) and Young's Modulus (E) are estimated from parameters that are sensitive to the fluid present in the pores of the rock.

It is concluded that Average Brittleness achieved from Grieser and Bray (2007) Equation is a relative measure. This information must be considered for the seismic inversion results analysis, where the brittleness was estimated from rock elastic properties obtained during the seismic inversion process. Figure 7 shows Average Brittleness estimated from well P-2 elastic properties. As expected, there are high brittleness values where Vsh is low. Furthermore, there are some intervals where Average Brittleness (Bri_avg) and shale Volume (Vsh) are high, this high brittleness is interpreted as due to more quartz content in the samples and, the water saturation estimation could be overestimated as a consequence of more clay content (Figure 4-a and 4-b).

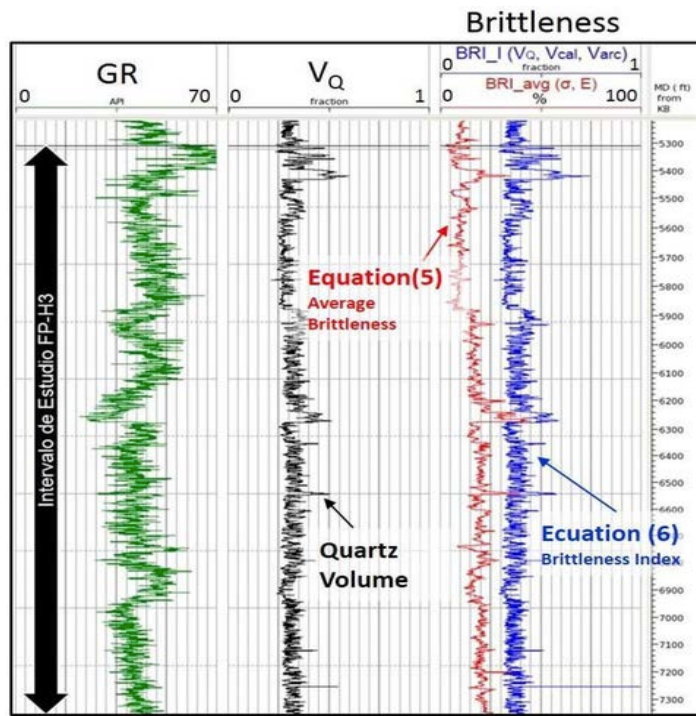


Figure 6. Estimated Brittleness in well P-5.

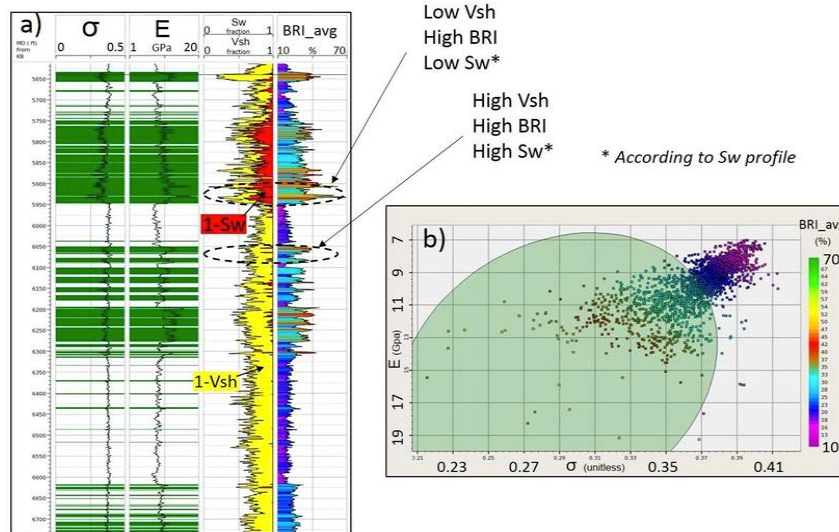


Figure 7: Average Brittleness (BRI_avg) estimated in well P-2. a) σ , E, Sw, Vsh and BRI_avg logs. b) Crossplot σ versus E colored by BRI_avg values. In (b) high brittleness values are green shaded, these values are highlighted in green also in the σ and E properties logs (a).

To perform an integrated analysis in the study target interval (FP-H3), diverse elastic properties were considered ($\lambda\rho$, $\mu\rho$, Zp and σ) and included in a same crossplot (Figure 8). A petrophysical evaluation for the different wells was added to this analyses, to accomplish a better understanding of the rock physics related to the reservoir.

Comparing Figures 5 and 8, there is a correlation between Quartz Volume increase and Average Brittleness (BRI_avg) increase. Interpreting Figure 8, it is possible to get a discrimination for Brittleness using the Lambda-Rho ($\lambda\rho$) versus Mu-Rho ($\mu\rho$) crossplot.

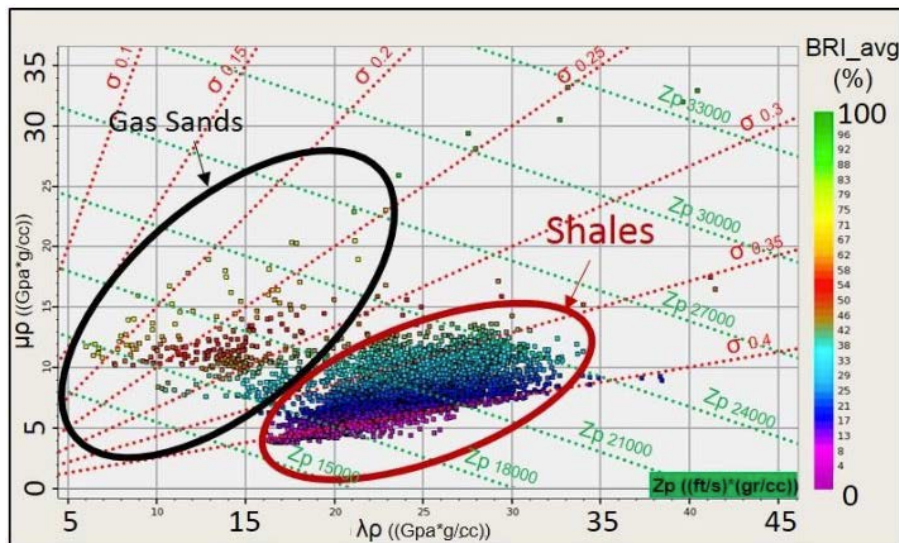


Figure 8. Crossplot $\lambda\rho$ vs $\mu\rho$, FP-H3 interval, P-4 and P-5 wells. Colored samples by Average Brittleness (BRI_avg). The plot also shows the constant values for σ and Zp .

When we observe the answer associated to different lithologies and fluids for the FP-H3 interval, we note that a rock is more compressible as it has more gas content and, as a consequence, it would have lower values of $\lambda\rho$. Furthermore, high gas saturations are related to higher sand content given that this fact means higher porosity. On the other hand, as the clay content increases, $\mu\rho$ values are lower, due to the low rigidity that characterizes the shales.

After all the analyses were completed, there is evidence that the rock Brittleness is related to its quartz volume. Two samples with the same brittleness could have different LMR values, depending on how is the quartz disposed in the rock. The sandstone laminar disposition has more porosity and permeability than the siltstone and a better gas saturation, making it more compressible, that means lower Lamé impedance values ($\lambda\rho$ y $\mu\rho$).

Brittleness is a property that has been used for shale characterization in many studies, looking to identify the best candidates for hydraulic fracturing, for gas production. For the target interval FP-H3, it was possible to discriminate ductile shales from brittle ones using crossplots Lambda-Rho ($\lambda\rho$) versus Mu-Rho ($\mu\rho$) (Figures 5 and 8).

To obtain more gas production from the shales, improving the permeability beyond the matrix permeability is necessary. Even with good permeabilities from natural fractures, hydraulic fracturing is needed to obtain successful production results (Kundert and Mullen, 2009).

The studied interval FP-H3 shows low permeabilities (nano-millidarcy order), so that the selection of the most brittle intervals to be

fractured is determinant to the gas production in enough quantity to be commercial.

The brittleness concept for a rock involves Poisson ratio (σ) and Young's modulus (E). These two components are combined to reflect the capacity that the rock has for failing as a consequence of a strain (Poisson ratio) and to maintain the fracture after breaking (Young's modulus). The ductile shales are not good reservoirs because the natural or hydraulic fractures will tend to close, even though, the ductile shales represent a very good seal. While the brittle shales are more prone to natural fracturing and it is more probable that responds favorably to hydraulic fracturing. These are the reasons why is important to quantify the brittleness combining both mechanical properties (σ and E) (Rickman et al., 2008).

The Porquero geologic characteristics, as well as the short production tests in five intervals for well P-2, indicate that to develop the condensate gas discovered in the area is necessary the application of stimulation techniques that allow improving the low natural permeability in the formation. With the purpose of technical feasibility and economic evaluation, it was designed a hydraulic fracturing pilot test in well P-2 (Leyva et al., 2012).

In Figure 9, crossplots of Lambda-Rho ($\lambda\rho$) versus Mu-Rho ($\mu\rho$) and well logs in the target interval for well P-2 are shown. For the crossplots and well logs, the proven intervals and/or fractured are indicated (1, 2, 3 and 4). The $\lambda\rho$ and $\mu\rho$ logs are colored with green and red stripes highlighting the most brittle zones in the studied section, according to the selection done using the crossplot in Figure 7.

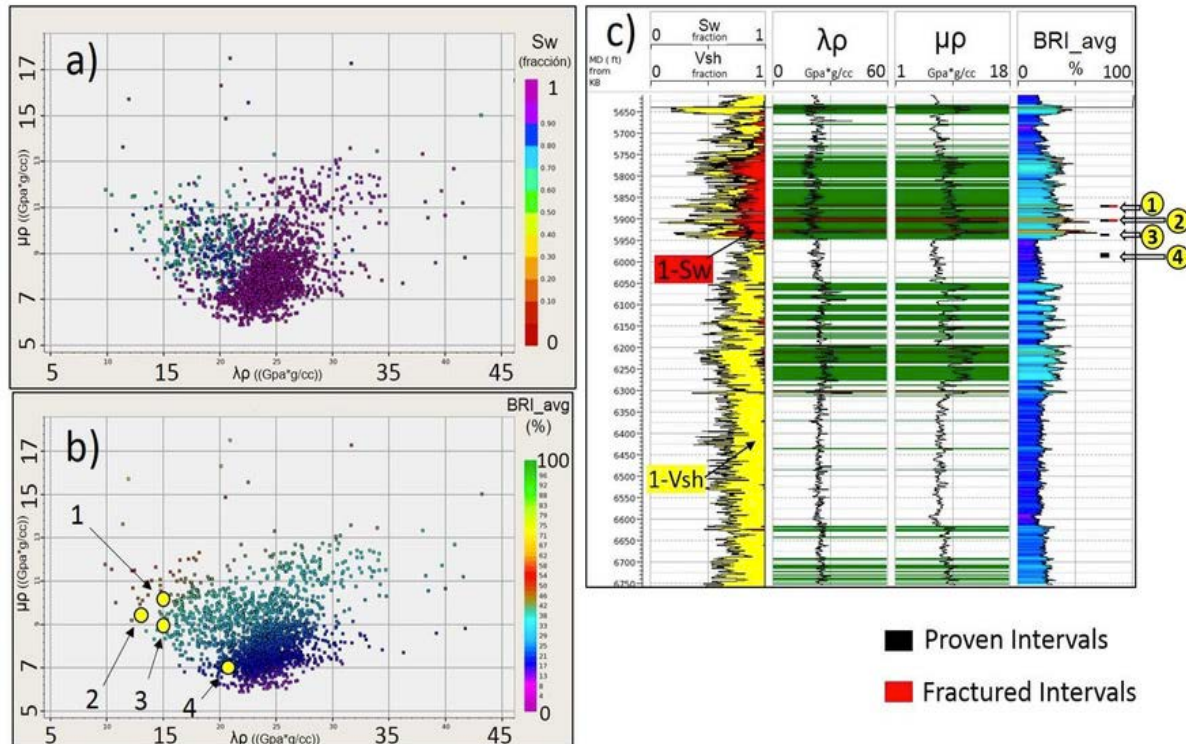


Figure 9: Proved Intervals in FP-H3, well P-2. Plots $\lambda\rho$ versus $\mu\rho$ for the interval FP-H3, a) Sw colorbar and b) coloured by BRI_avg ; yellow circles indicate proven intervals in the well. c) Sw , Vsh , $\lambda\rho$, $\mu\rho$ and BRI_avg logs showing proving and/or fracturing intervals in the P-2 well.

Thanks to fracturing, the productivity index (PI) was tripled compared to the initial test. In the initial test (without fracturing) the labeled intervals in Figure 9, were produced jointly combined with a fifth shallower interval that is out of the scope of this analysis. In the post-fracturing test the fracturing intervals 1 and 2 produced jointly with intervals 3 and 4 that were not fractured.

In the brittleness log as in the crossplots, we observe that the selection of the intervals to be fractured was good, because they have the lowest S_w (Water Saturation) according to the petrophysical evaluation (Garcia, 2014). In the 6050 - 6275 ft (MD) and 6700 – 6750 ft (MD) intervals, favorable brittleness are observed even with the high values of S_w .

Simultaneous Seismic Inversion

Simultaneous seismic inversion was carried out to obtain estimates of P-wave Impedance, S-wave Impedance and Density, using angle gathers and the Aki-Richards equation as proposed by Fatti et al. (1994), which can be used to predict lithological and fluid properties in the subsurface (Hampson et al., 2005).

In a simultaneous seismic inversion, the seismic data is inverted simultaneously in volumes of elastic properties (Z_p , Z_s and ρ), that allow better estimation of lithologic distribution, porosity and hydrocarbon saturation (Filippova et al., 2011). The simultaneous inversion process, including rock physics constrained, reduces the no uniqueness of the inversion which allows achieving a stable process.

In Figure 10, the results of the simultaneous seismic inversion can be observed. The achieved computation of P-wave Impedance (Z_p), S-wave Impedance (Z_s) and Density (ρ) are shown for P-2 well.

From the rock physics analysis, we determined that the crossplot Lambda-Rho ($\lambda\rho$) versus Mu-Rho ($\mu\rho$) represents an excellent tool for discriminating rock quality and kind of fluid. This graph can be used for the quantitative interpretation of seismic inversion results.

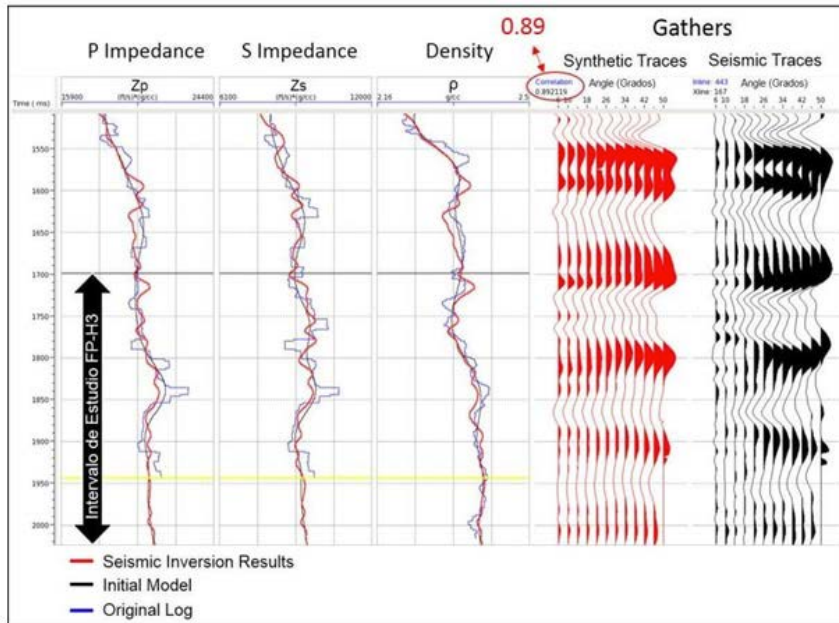


Figure 10: Simultaneous Seismic Inversion Results – data surrounding well P-2.

Figure 11 shows three crossplots Lambda-Rho ($\lambda\rho$) versus Mu-Rho ($\mu\rho$), derived from the seismic inversion responses and well data information. This figure summarizes the rock physics and seismic inversion results, and it is going to be decisive for geobodies definition. The integration of well and seismic data are shown in a crossplot (figure 11-c), where there is a polygon designed to define geobodies in the FP-H3 interval (highlighted in yellow). This selection was done with the purpose of defining the anomalies associated to a high gas content, sandstones with lower clay content, high lamination intervals and shales with high quartz content. At this stage, the discrimination completed using the Average Brittleness was determinative in the polygon selection.

The inversion anomalies obtained from the definition of an area or illuminated zone in the crossplot Lambda-Rho ($\lambda\rho$) versus Mu-Rho ($\mu\rho$) were interpreted to define geobodies (Figure 11). These areas consider lithology, brittleness, gas saturation and thickness (considering the ability to be resolved by the scaled data to seismic frequencies). These defined zones are assumed to constitute the geobodies that represent elastic properties related to lithologic and fluid conditions defined during the rock physics analysis. It is important to consider the possible lamination, in some zones, during the analysis of the seismic inversion results.

Figure 12 shows the extracted geobodies obtained from the elastic properties resulting from the seismic inversion, where each color corresponds to a subinterval inside FP-H3.

Finally, these anomalous zones, represented by geobodies, were populated with different elastic properties achieved through the seismic inversion process to understand and visualize the properties behavior inside each geobody and relate them to rock quality and fluid presence.

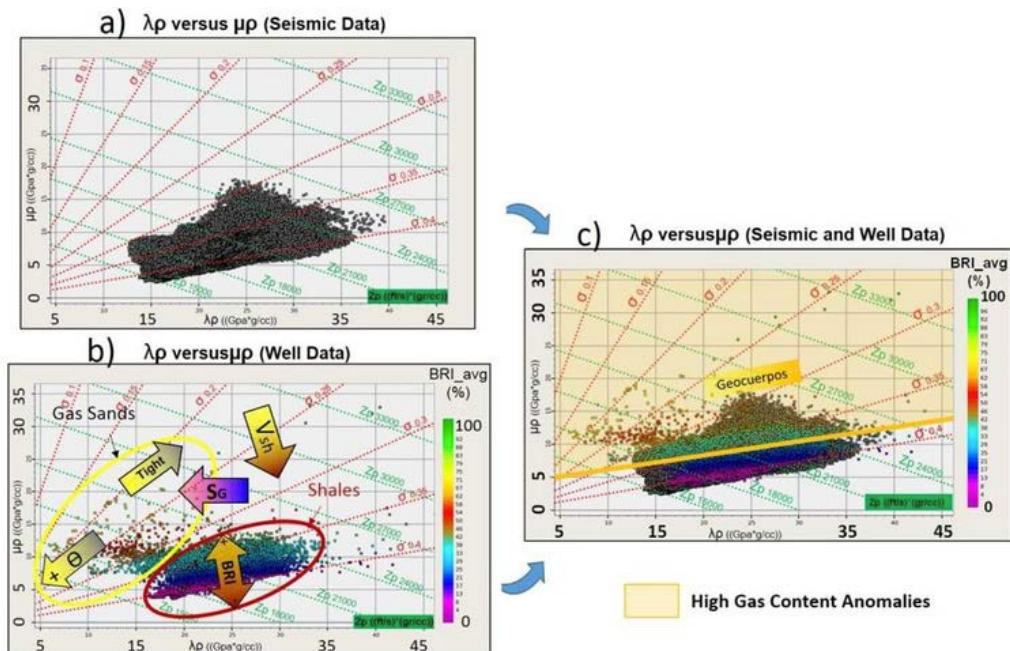


Figure 11: Resulting properties, seismic inversion and well data, interval FP-H3: a) crossplot $\lambda\rho$ versus $\mu\rho$ constructed from seismic inversion results; b) crossplot $\lambda\rho$ versus $\mu\rho$ generated from well data (P-1, P-2, P-3, P-4 and P-5), colors correspond to Average Brittleness (BRI_avg) estimated from elastic properties. Gas saturation (Sg=1-Sw), Vsh, Θ and BRI_avg trends are shown; c) crossplot with integrated seismic and well data, in yellow, the designed polygon to define the geobodies in the FP-H3 interval (cutoff). Constant values of σ are shown (red dotted lines) and Z_p (green dotted lines).

Among the properties used to populate the geobodies, according to the obtained results during the rock physics analysis, brittleness represents the property that allows having a better discrimination of the reservoir and it is the best indicator of the intervals that could respond favorably to a hydraulic fracture. For the brittleness estimation, properties E and σ were calculated by using the seismic inversion output and Equation (5), where maximum and minimum values for Poisson ratio and Young's Modulus were defined (from seismic inversion) in the FP-H3 target interval, so Average Brittleness is a relative measure. That is why the next relationship is valid only for the Average Brittleness calculation, derived from the seismic inversion results in the target interval of the study area:

$$BRI_{avg_S} = 134.974 - 337.838 * \sigma + 3.374 * E. \quad (7)$$

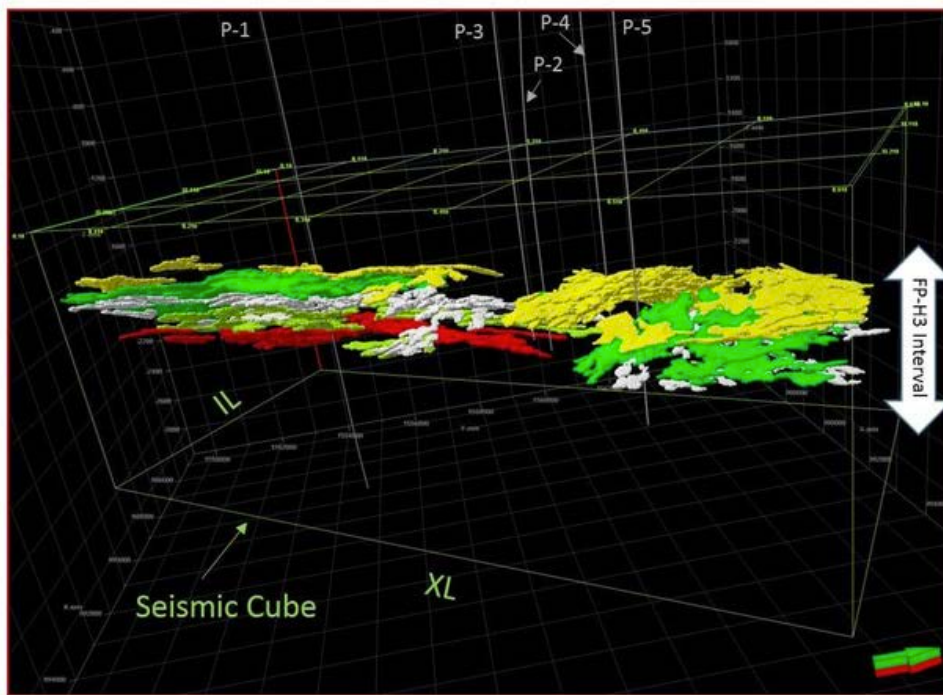


Figure 12: Resulting geobodies for interval FP-H3, 3-D View.

For a sample the estimated average brittleness (BRI_{avg}) from well data differs in magnitude from seismic inversion average brittleness computed (BRI_{avg_S}), although the measure corresponds to the same sample. The reason for this difference is in the discrepancy between maximum and minimum values used for the brittleness computation in each case.

Geobodies were defined based on favorable criteria for reservoir rocks with high gas saturations; nevertheless, it is possible to define for each geobody, the zones with the best reservoir conditions from their properties $\lambda\phi$, $\mu\phi$, Z_p , Z_s , brittleness, etc.

Figure 13, shows the 3D view of one of the geobodies within the FP-H3 interval, in the seismic volume, named FP-H30-I. This geobody was populated with the Average Brittleness (BRI_{avg_S}) and intersected by a plane close to the well P-2, which allows us to observe vertical and lateral brittleness changes. In the upper left part of the Figure 13, the petrophysical evaluation (Garcia, 2014) results and the elastic properties logs calculated for the well are shown. The calculated high brittleness interval in P-2 using the logs (BRI_{avg}) matches with the high brittleness interval estimated from the seismic inversion response (BRI_{avg_S}).

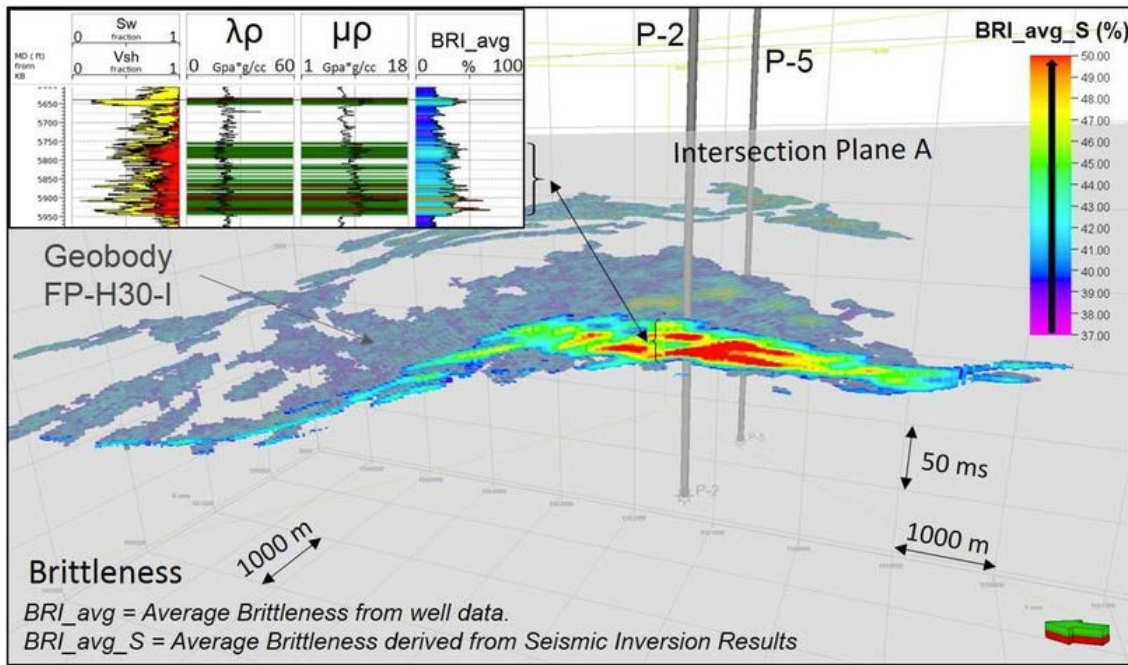


Figure 13: 3D View: Geobody FP-H30-I populated with BRI_avg_S, the geobody is intersected by the plane A. In the upper left corner there are the results of the Sw and Vsh properties estimation, followed by $\lambda\rho$, $\mu\rho$ and BRI_avg for well P-2.

Conclusions

- The target interval is defined by low lateral continuity laminar sandstones with low permeability (nano- milidarcy order), that are grouped in multiple cycles, embedded in very thick shale intervals. Despite these features and the vertical seismic resolution limit, it was demonstrated that an appropriated solution allows an ideal reservoir characterization from seismic data, to achieve an optimal reservoir production.
- Quantitative seismic interpretation resulting from well logs, seismic inversion and rock physics analysis give a better understanding of the behavior of the different reservoir units inside the target interval. The present study gives the opportunity to include smaller rock grains reservoirs into the field model. This observation involves a revision of petrophysical evaluations, horizons interpretation and volumetric resources estimation.
- A methodology is proposed for FP-H3 reservoir characterization, where sandstones, laminar sands, siltstones and shales with high quartz content are included. Rock physics analysis, seismic inversion and brittleness estimation are important steps in the used workflow.
- Rock physics analysis performed in wells leads to a quantitative interpretation of seismic inversion results that gave geobodies maps for five sublevels inside FP-H3 interval (the reservoir in the area), as final output. Maps show different elastic properties values that make possible classifying geobodies by zones.
- Shales and siltstones with high quartz content were included to the total rock volume in the target interval FP-H3 in the Porquero

Formation which is an important complement to the reservoir prospectivity, given that clayish lithologies could contribute to gas production in the field.

- Crossplots Lambda-Rho ($\lambda\rho$) versus Mu-Rho ($\mu\rho$) and petrophysic available data allow for differentiating gas sands from shales. Using mineralogic logs, it was possible to get shale discrimination according its quartz content.
- Rock brittleness was estimated from Poisson ratio (σ) and Young Modulus (E) using the Grieser and Bray (2007) Equation. Mineralogical information from logs indicates that brittleness computed from elastic properties for shales and siltstones is strongly linked to the quartz content.
- There is a strong correlation between brittleness estimated using mineralogic logs, methodology proposed by Jarvie et al. (2007), and average brittleness computed using log calculated elastic properties (σ and E), through Grieser and Bray (2007) Equation.
- Cores, petrophysical evaluation, mineralogical and image logs joined to brittleness values and crossplots Lambda-Rho ($\lambda\rho$) versus Mu-Rho, allowed the definition of trends or zones in Lambda-Rho ($\mu\rho$) versus Mu-Rho graphic related to rock quality and fluids for the target interval FP-H3.
- Due to the reservoir properties it is mandatory to use hydraulic fracturing to produce it. The results obtained in this study from the selection of zones with higher brittleness allow defining the best intervals to be fractured in the wells and in the area using 3D seismic.
- In FP-H3 interval, higher brittleness zones are related to shales and siltstones with high quartz content and laminar sandstones. These are the zones that define the reservoir.
- Using different elastic and petrophysical properties in the same crossplot allowed us achieving an integrated analysis of rock physics and geobodies selection (sweet-spots).

References

- BETANCOURT, J., ARMINIO, J., GARCÍA, E., y YORIS FRANKLIN, 2015, Modelo Petrofísico Integrado, herramienta clave para la detección de yacimientos de gas condensado en capas delgadas y de baja permeabilidad. Cuenca del Valle Inferior del Magdalena, Colombia. Congreso Mexicano del Petróleo, Guadalajara 2015.
- BIOT, M., 1956, Theory of propagation of elastic waves in a fluid-saturated porous solid. The Journal of the Acoustical Society of America.
- CORE LABORATORIES, INC., 2011, X-Ray Diffraction Analysis, Pacific Stratus, P-2 Well, Colombia, South America.
- FATTI, J. L., SMITH, G.C., VAIL, P.J., STRAUSS, P.J., and LEVITT, P.R., 1994, Detection of gas in sandstone reservoirs using AVO analysis: a 3D Seismic Case History Using the Geostack Technique": Geophysics, vol. 59, p. 1362-1376.
- FILIPPOVA, K., KOZHENKOV, A., and ALABUSHIN, A., 2011, Seismic inversion techniques: choice and benefits. Special Topic: Unconventional

Resources and the Role of Technology. First Break. European Association of Geoscientists and Engineers.

GARCÍA, E., 2014, Actualización de la evaluación petrofísica de arenas apretadas de Porquero. Pacific Rubiales Energy Corp. Informe Interno.

GASSMANN, F., 1951, Über die elastizität poroser medien: Vierteljahrsschr. Der Naturforsch. Gesellschaft Zurich.

GHOSH, S., DI LUCA, M., AZUAJE, V., y BETANCOURT, J., 2013, Marco Estratigráfico-Sedimentológico, Valle Inferior del Magdalena, Colombia. Pacific Rubiales Energy. Informe Interno. GOODWAY, B., 2014, The Magic of Lamé. Recorder. Canadian Society of Exploration Geophysicists (CSEG).

GOODWAY, B., CHEN, T., and DOWNTON, J., 1997, Improved AVO fluid detection and lithology discrimination using Lame petrophysical parameters; lr , mr & l/m fluid stack, from P and S inversions. Society of Exploration Geophysicists (SEG) 1997 Annual Meeting.

GOODWAY, B., 2007, A tutorial on AVO and Lamé constants for rock parameterization and fluid detection.

GOODWAY, B., PEREZ, M., VARSEK, J., and ABACO, C., 2010, Seismic petrophysics and isotropic-anisotropic AVO methods for unconventional gas exploration.

GRIESER, B., and BRAY, J., 2007, Identification of Production Potential in Unconventional Reservoirs. Society of Petroleum Engineers (SPE), Production and Operations Symposium. HAMPSON, D., RUSSELL, B., and BANKHEAD, B., 2005, Simultaneous Inversion of Pre-Stack Seismic Data. Society of Exploration Geophysicists (SEG) 2005 Annual Meeting.

HERWANGER, J., BOTTRILL, A., and MILDREN, S., 2015, Uses and Abuses of the Brittleness Index With Applications to Hydraulic Stimulation. Unconventional Resources Technology Conference (URTeC).

HILTERMAN, F., 2001, Seismic Amplitude Interpretation. SEG-EAGE distinguished Instructor Series, N° 4, Geophysical Development Corporation.

JARVIE, D., HILL, R., RUBLE, T., and POLLASTRO, R., 2007, Unconventional shale-gas systems: The Mississippian Barnett Shale of North-Central Texas as one model for thermogenic shale-gas assessment: AAPG Bulletin, 91, 475–499.

KUNDERT, D., and MULLEN, M., 2009, Proper Evaluation of Shale Gas Reservoirs Leads to a More Effective Hydraulic-Fracture Stimulation. Society of Petroleum Engineers (SPE).

LESPINASSE, D., 2006, Estudio de factibilidad del uso de Atributos de Impedancia Elástica Pp y Ps para la discriminación litológica y de fluidos utilizando "Closest Match Diffusion Algorithm" (Bloque Sur, Guafita). Trabajo de grado, Universidad Simón Bolívar.

LEYVA, I., ARMINIO, J., VEGA, R., LUGO, J., AND DASILVA, A., 2012, Exploración de Plays no Convencionales para Gas en la Formación Porquero de la Cuenca del Valle Inferior del Magdalena, Colombia. XI Simposio Bolivariano - Exploración Petrolera en las Cuencas Subandinas.

MAVKO, G., MUKERJI, T., and DVORKIN, J., 1998, The Rock Physics Handbook. Tools for Seismic Analysis of Porous Media. Cambridge University Press.

PÉREZ, R., and MARFURT, K., 2015, Identification of brittle/ductile areas in unconventional reservoirs using seismic and microseismic data: Application to the Barnett Shale. Society of Exploration Geophysicists (SEG). Interpretation.

REYES-HARKER, A., MONTENEGRO, G., y GÓMEZ, P., 2000, Evolución Tectonoestratigráfica del Valle Inferior del Magdalena, Colombia. VII Simposio Bolivariano - Exploración Petrolera en las Cuencas Subandinas.

REYES, J., MANTILLA, M., y GONZÁLEZ J., 2000, Regiones Tectono-Sedimentarias del Valle Inferior del Magdalena, Colombia. VII Simposio Bolivariano - Exploración Petrolera en las Cuencas Subandinas.

RICKMAN, R., MULLEN, M., PETRE, E., and KUNDERT, D., 2008, A Practical Use of Shale Petrophysics for Stimulation Design Optimization: All Shale Plays Are Not Clones of the Barnett Shale. Society of Petroleum

Engineers (SPE).

RUSSELL, B., 2014, Prestack Seismic Amplitude Analysis: An Integrated Overview. Interpretation, Vol. 2 No 2. Society of Exploration Geophysicists (SEG).

ZHANG, B., ZHAO, T., JIN, X. AND MARFURT, K. 2015, Brittleness evaluation of resource plays by integrating petrophysical and seismic data analysis. Society of Exploration Geophysicists (SEG). Interpretation

Professional career of the author and co-authors:

Mario Di Luca Vingelli (Author): Mario Di Luca received his undergraduate degree (2001) in Geophysics Engineering from the Universidad Central de Venezuela and a MSc. in Geophysics (2017) from Universidad Nacional de Colombia, where the thesis focused on characterizing a heterogeneous reservoir through the estimation and analysis of elastic properties resulting from seismic inversion. He has 17 years working experience in the E&P Oil and Gas Industry, with technical responsibilities in acquisition and interpretation of seismic data of fields in Western Venezuela, Burgos Mexican and Colombian Basins. He is currently working as a Geophysics Senior Specialist at Frontera Energy Corp., in Bogota, Colombia.

Trino Salinas (Co-author): Trino Salinas G. received a MSc. in geophysics from Colorado School of Mines (1997) and has 28 years of work experience at the oil & gas industry with local and international companies such as Ecopetrol, Saudi Aramco and Fronteras Energy, working as part of the geoscience teams. He is a specialized geophysicist in seismic imaging, and quantitative seismic interpretation based on rock physics using well logs and 3D/4D seismic data. He was responsible for testing and proving the 4D/3C seismic monitoring effectiveness at an in-situ combustion experimental project for heavy oil at the Colombian Llanos basin, to identify flow patterns.

Roderick Pérez (Co-author): Roderick Pérez completed his undergraduate degree in Geophysical Engineering at the Universidad Simon Bolívar (Venezuela) in 2007, a M.S. in Geology (2008) and Ph.D. in Geophysics (2013) at OU, and currently, he is pursuing a MBA program at the Universidad de Los Andes (Colombia). Dr. Pérez has experience in several companies such as Noble Energy, Anadarko Petroleum, DrillingInfo, and Pacific Exploration & Production. Additionally, he is teaching at the Universidad Nacional de Colombia the Seismic Stratigraphy course. Currently, he is working as Senior Geophysical Advisor for several oil companies in Latin America, specialized in the generation and interpretation of seismic attributes for conventional and unconventional reservoirs.



Geo-Predicción: Inversión Simultánea en Impedancia y Facies Sísmicas para Caracterizar Contenido de Roca/Fluido en Yacimientos de Carbonatos

Dante Granados, Alejandro Salas (PEMEX), Adrien Caudron, Marco Vázquez (APOGEE), Alan Mur, Gabriela D'Aubeterre, Simón Payne (IKON)

CMP2018_GC78
Artículo presentado
en el CMP / 2018

● Resumen

El Sureste de México está compuesto por formaciones carbonatadas de alto interés para la producción de hidrocarburos en la región, principalmente formaciones de carbonatos dolomitizados que contienen aceite ligero. La profundidad a la que se encuentran estos yacimientos está alrededor de los 6,300m a 7,000m, con un espesor variado que puede ir desde los 50m hasta 150m.

La caracterización de estos yacimientos se convierte en un reto para los tomadores de decisiones, y éste es solucionado mediante la integración de información geológica, geofísica e información de producción del área de interés.

El trabajo aquí presentado muestra la implementación y resultados del algoritmo de inversión sísmica Ji-Fi (Joint Inversion – Facies Inversion) en un campo con formaciones dolomitizadas y que presenta las condiciones peculiares del Sureste de México. Ji-Fi es un algoritmo de inversión sísmica que considera en su solución los fenómenos discretos (facies) y continuos (impedancia en función de las facies) que son parte de la inversión sísmica. Por lo tanto, los resultados obtenidos son una representación más precisa del fenómeno ocurrido en el subsuelo.

Introducción

La base de esta solución se encuentra en el principio de que cada impedancia observada (fenómeno continuo) es resultado de un cambio de facies (fenómeno discreto).

Caso contrario a las soluciones comunes, las cuales limitan la relación entre impedancias y facies con base en un modelo de baja frecuencia, es decir, que son soluciones que únicamente consideran la parte discreta del fenómeno (facies), a partir de una tendencia de valores.

El riesgo de limitar el fenómeno de la impedancia sísmica a un modelo de baja frecuencia, es el de obtener resultados que no sean una representación propia del subsuelo. Este riesgo es imprescindible partiendo de las siguientes premisas:

1. Los valores iniciales del modelo de baja frecuencia (AI_0, SI_0 y r_0) son difíciles de determinar.
2. El modelo de baja frecuencia se encuentra lejos de ser una representación de los eventos sísmicos, generando una tendencia matemática sobre el resultado final.

Para sobrellevar dicho problema se ha desarrollado la solución Ji-Fi, donde AI_0, SI_0 y r_0 son especificadas para cada facie de manera individual, en vez de generar tendencias de valores para un modelo de baja frecuencia.

Una vez definidos los valores AI_i, SI_i y r_i por facie, es posible resolver el problema de inversión sísmica considerando los fenómenos discretos (facies) y continuos (impedancias en función de las facies), que forman parte del problema mediante una solución bayesiana al problema de inversión sísmica.

Como resultado se obtendrán valores AI_i, SI_i y r_i con mayor sentido sísmico-geológico, los cuales sustentan los resultados de una interpretación cuantitativa (por ejemplo, correlación entre modelos petrofísicos y modelos de física de rocas) y cualitativa (por ejemplo, correlación entre cimas y horizontes sísmicos).

Caso estudio – Sureste de México

El caso estudio presentado se enfoca en un yacimiento con evidencias y producción de aceite ligero en carbonatos dolomitizados. La profundidad (6,300m y 7,000m) y espesor (50m a 150m) de dichos carbonatos es coincidente con las evidencias

geológicas que existen en la región. El campo de interés cuenta con cobertura sísmica en toda su área de extensión (resolución sísmica \leq 200m), al igual con pozos productores (4 pozos) y no productores (7 pozos secos y/o invadidos).

La información anterior fue insumo del algoritmo de inversión sísmica Ji-Fi, cuyos resultados permitieron llegar a una clasificación de facies con cambios laterales consistentes y geológicamente coherentes.

Gráficas

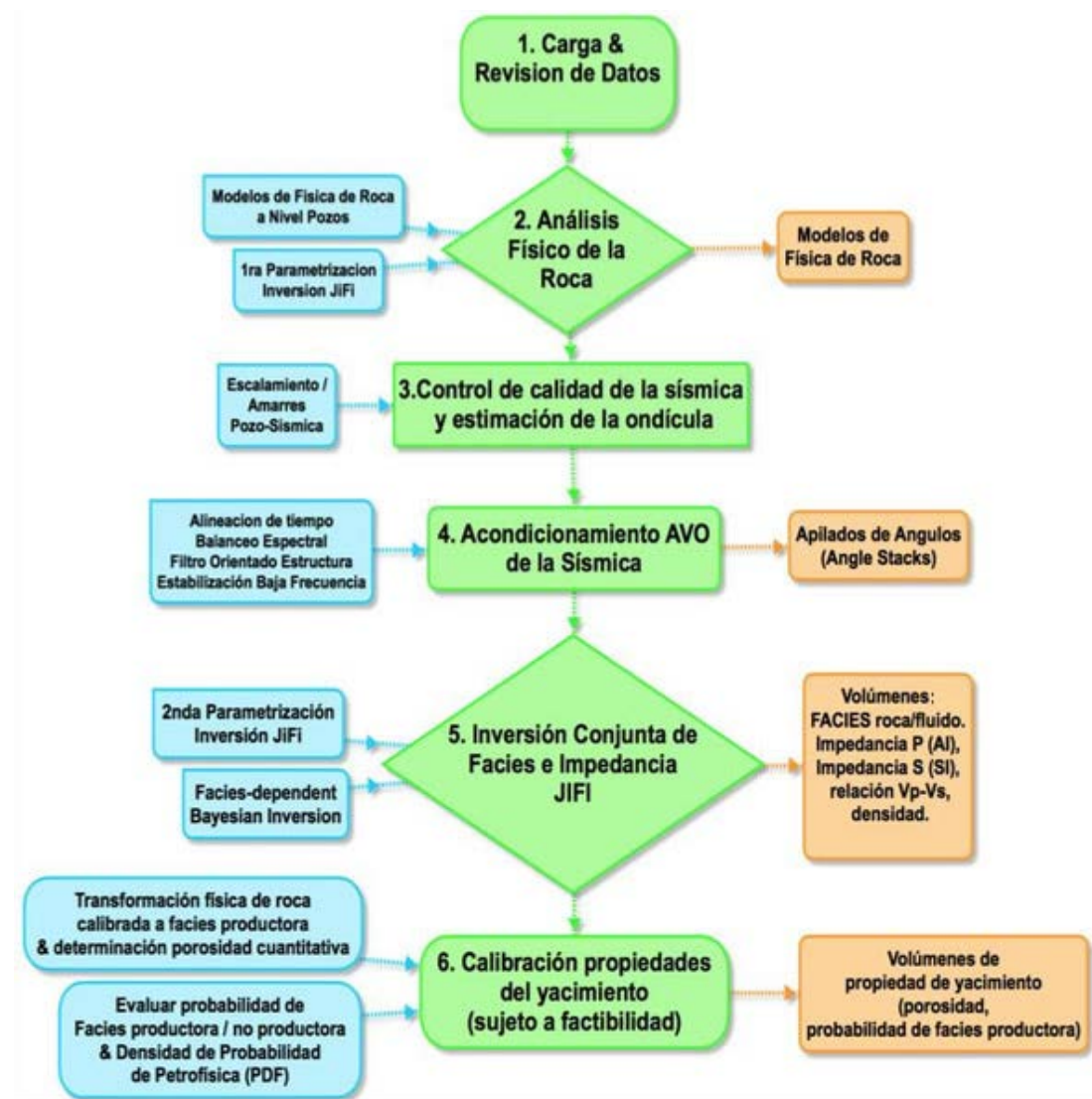


Ilustración 1. Flujo de trabajo Ji-Fi.

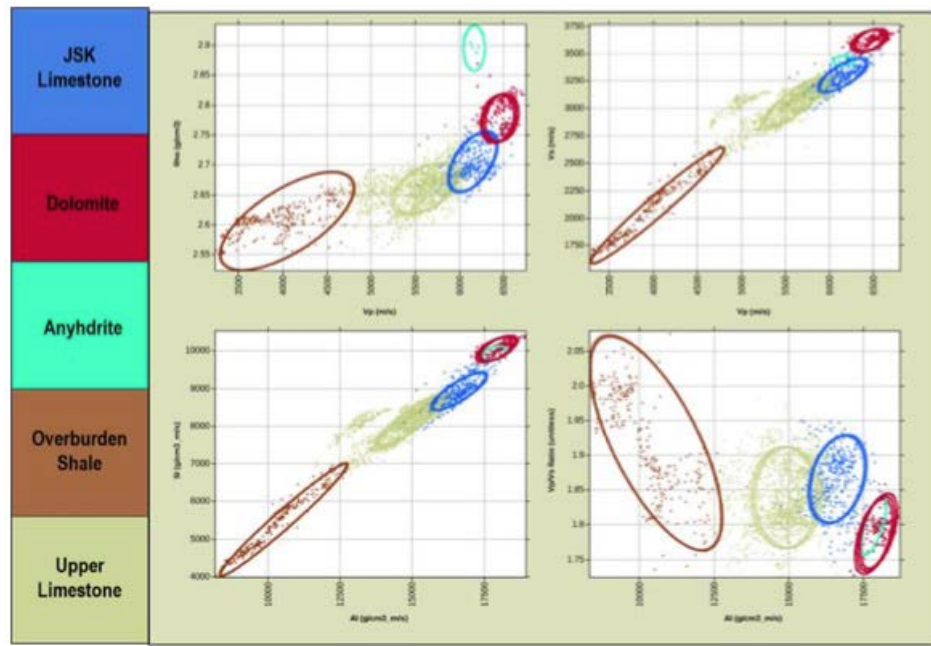


Ilustración 2. Evaluación de propiedades elásticas y clasificación por facies. Caso de estudio SE de México.

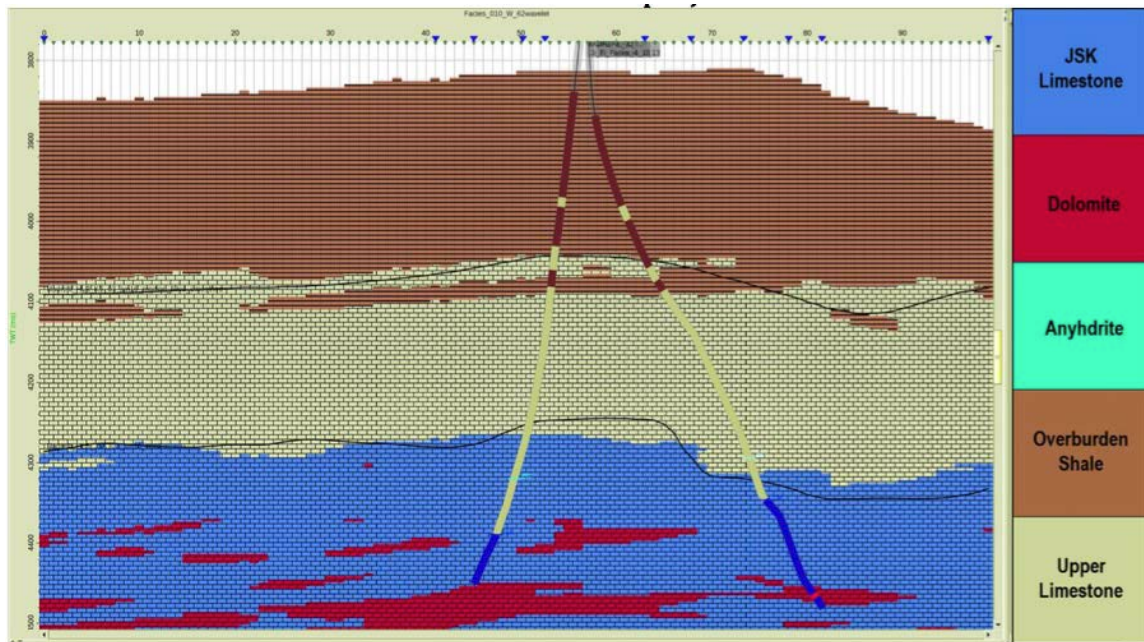


Ilustración 3. Distribución de facies estimadas por Ji-Fi. Caso estudio SE de México.

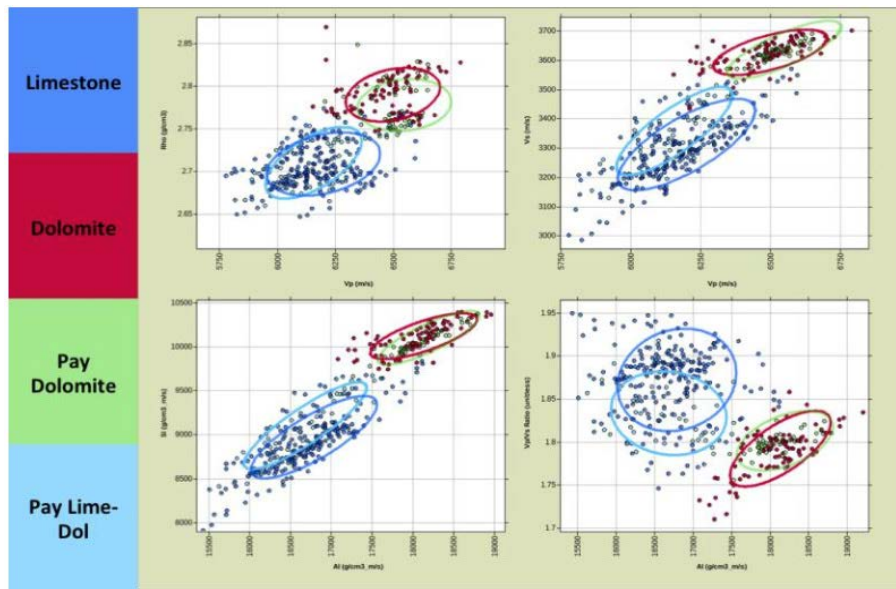


Ilustración 4. Evaluación de propiedades elásticas y clasificación de facies de interés y su contenido de fluido. Para dicha discriminación se consideró valor de porosidad >2%.

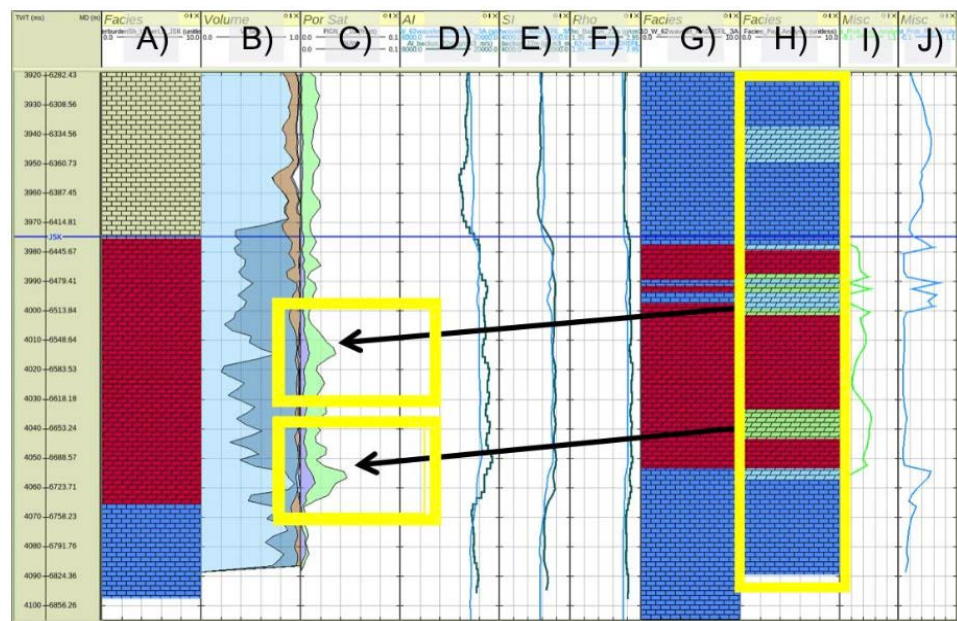


Ilustración 5. Evaluación petrofísica y comparación de facies estimadas por Ji-Fi y análisis de contenido de fluido. Columnas: A) Facies, B) Volumen, C) Porosidad/Saturación, D) I_A , E) I_S , F) Facies Ji-Fi, G) Facies análisis de contenido de fluido, H) Probabilidad Facie Pay Dolomite, I) Probabilidad Facie Pay Lime Stone.

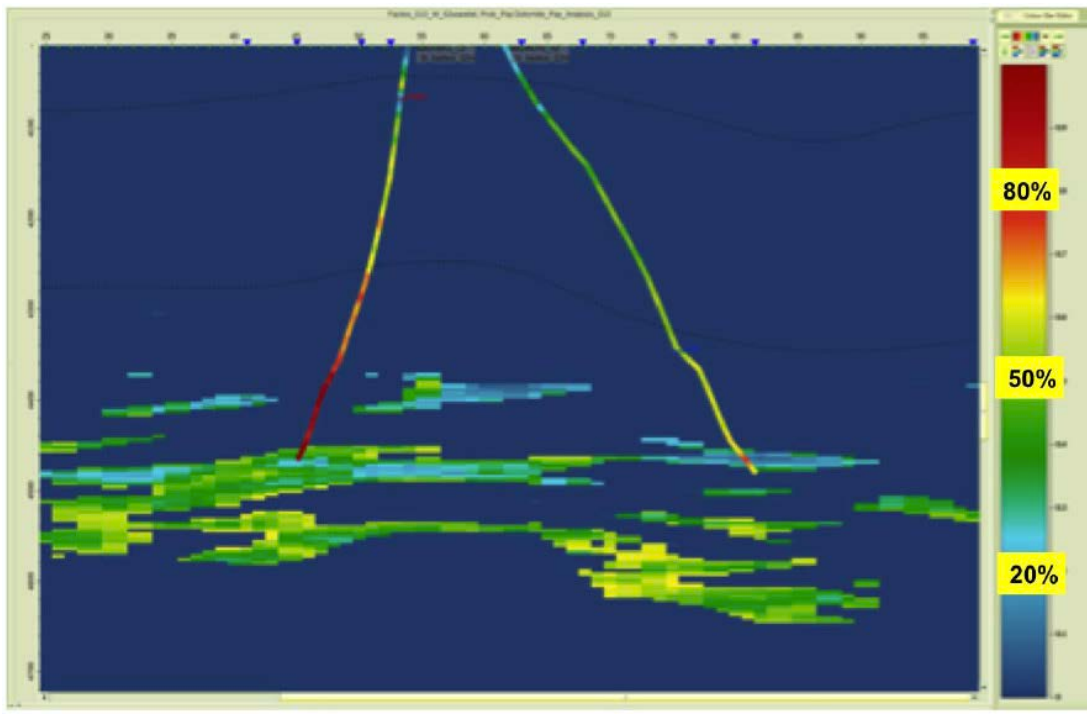


Ilustración 6. Distribución de facies en función de su probabilidad de concurrencia a partir del análisis de contenido de fluido.

Conclusiones

El enfoque de inversión sísmica que se describe en el flujo de trabajo propuesto es Inversión conjunta de facies e impedancia. El enfoque Ji-Fi es una inversión bayesiana realizada en los datos apilados por ángulos y que posee los siguientes beneficios:

1) No se requiere un modelo de baja frecuencia convencional.

Otros enfoques de inversión sísmica requieren un modelo de baja frecuencia para compensar la información no presente dentro del ancho de banda sísmico. La construcción de estos modelos de baja frecuencia requiere mucho tiempo y es vulnerable a generar un sesgo en los resultados finales de la inversión.

El enfoque Ji-Fi evita estos problemas mediante el desarrollo iterativo del modelo de baja frecuencia a partir de un conjunto de tendencias de la física de la roca que describen las propiedades elásticas de las facies individuales.

Las actualizaciones a la inversión basadas en nuevos datos de pozos pueden hacerse mucho más rápidamente usando el enfoque Ji-Fi, ya que todo lo que se requiere es una revisión de las tendencias de física de roca.

2) Mayor uso de la información de física de las rocas de registros de pozos.

Los modelos de física de roca por cada una de las facies litológicas de interés son insumos del algoritmo de inversión Ji-Fi y como resultado de la inversión Ji-Fi se obtiene al mismo tiempo y en un solo paso los volúmenes de Impedancia I_p / I_s , volúmenes de Facies Sísmicas con sentido

geológico, y sin tener que aplicar ningún proceso matemático post-inversión.

3) Un aumento aparente de la resolución sísmica

El aumento aparente en la resolución también viene del enfoque mejorado para construir el modelo de baja frecuencia. Un ejemplo se muestra en la Figura 1. El desenfoque (smearing) de la información de baja frecuencia en el enfoque convencional, resulta en un efecto de halo para el evento correspondiente en la arena con salmuera y alrededor de los yacimientos de arenisca de gas objetivo. Por el contrario, la estimación exacta de la información de baja frecuencia utilizando el método Ji-Fi resulta en capas mejor definidas.

Nomenclaturas

Ji-Fi: Joint Inversion – Facies Inversion (marca registrada)

AI_o : Impedancia acústica (onda p) observada

SI_o : Impedancia de cizalla (onda s) observada

r_o : Densidad observada

Agradecimientos

Agradecimientos al Activo Integral de Producción Bloque Sur – 03, a la Gerencia de Aseguramiento Tecnológico de Exploración y Producción, al equipo de trabajo de Ikon Science en Houston, y a todos que de manera voluntaria apoyaron con comentarios a la realización de este trabajo.

Referencias

Evolución geológica del sureste mexicano desde el Mesozoico al presente en el contexto regional del Golfo de México, Padilla y Sánchez, 2007

Joint Impedance and Facies Inversion – Seismic inversion redefined, Kemper, first break volume 32, September 2014

Trayectoria profesional del autor y coautores:

Autor

Adrien Caudron

M.Sc. Geología Ecole Nationale Supérieure de Géologie, Francia.
CEO y Co-fundador Apogee Geomodeling

Coautor

Dante Israel Granados Vázquez

Ingeniero Geólogo. Universidad Nacional Autónoma de México UNAM
Especialista Técnico B, Especialidad en Sedimentología y Estratigrafía, área Geociencias, en la coordinación de Diseño de Exploración, Activo Integral de Producción Bloque S03.

Alejandro Salas Valle

Licenciatura: Ingeniero Geólogo. Instituto Tecnológico de Ciudad Madero
Especialista Técnico, Gerencia de Aseguramiento Tecnológico de Exploración y Producción, Subdirección de Aseguramiento Tecnológico

Alan Mur

Doctor en Filosofía, Geología con especialidad en Geofísica
Geocientífico Sr, Ikon Science

Gabriela D'Aubeterre

Licenciatura: Ingeniero Geofísica, Universidad Simón Bolívar, Venezuela
Geocientífico Sr, Ikon Science

Simon Payne

Doctor en Filosofía, Geofísica y Sismología
Gerente Interpretación Cuantitativa, Ikon Science

Marco Vázquez (Expositor)

Licenciatura: Ingeniero Geofísico, Facultad de Ciencias de la Tierra, Universidad Autónoma de Nuevo León
Geofísico, Apogee Geomodeling



Elastic Reflection FWI for AVO and Long Length-Scale Parameter Estimations

Peng Shen (Chevron Energy Technology Company), Uwe Albertin (Chevron Energy Technology Company), and Anusha Sekar (Chevron Energy Technology Company)

CMP2018_GC27
Artículo presentado
en el CMP / 2018

● Summary

Conventional FWI uses diving waves for long scale velocity updates. Typical FWI applications are restricted to the acoustic wave propagation. It is debatable whether elastic FWI can bring any substantial added values to the conventional FWI. We show in this work that using the full orthorhombic elastic simulations and by including reflections into the elastic FWI, subject to proper chain rule, we are able to achieve not only short scale update but also the long scale update, both of which are required for the AVO inversion. We analyze two mechanisms for long scale update under the regime of elastic reflection FWI: local amplitude induced long scale domain of influence and an intrinsic tomography contained within FWI. The final example in 3D, targeted for sub-salt shear and compressional velocity determinations, demonstrates the robustness of the method, in which both of the aforementioned mechanisms are active.

Introduction

Conventional AVO analysis typically employs true amplitude imaging via Kirchhoff migration followed by Shuey and Zoeppritz equation-based analysis to recover elastic parameters. The latter requires picking of amplitudes from image gathers followed by computation of AVO gradients and intercepts, which often are limited in reliability, and are therefore aided by statistical analyses to improve the robustness of the procedure. As opposed to conventional image-based analysis, the AVO work can be posed as an optimization problem, which can be solved iteratively using quasi-Newton's methods. These methods use the objective functions and gradients which are linked directly to the seismic data. Here we formulate such an inversion through the use of 3D orthorhombic propagators, which extends conventional FWI to the orthorhombic elastic domain.

Mora (1988) show in two dimensions that by extending acoustic

to elastic FWI, reflection pressure data may be used to recover both p- and s- wave velocities or impedances at typical seismic imaging bandwidth. Recently Vigh et al. (2012) extend that work to three dimensions. Albertin (2015) showed that the 3D acoustic full waveform inversion in the reflection domain can be used to recover p-wave velocity information from pressure data with fairly high frequencies, to the order of 20Hz or more. The dominant effects of shear- mode conversion on pressure data are phase rotations and amplitude variations across the angle. A workflow consisting of an initial inversion for pressure wave velocity at shorter offsets, followed by an inversion for shear velocity at wider offsets, may be a reasonable scheme for the multi-parameter estimation (Sears et al., 2010). Albertin et al. (2016) adopt a similar separation scheme in 3D for orthorhombic media.

Here we pose the AVO related inverse problem as a simultaneous multiparameter inversion for p- and s- wave velocities excluding density. Our method uses reflection data which are of relatively high frequency. Interestingly, we observe that the method is effective at recovering relatively long length scale updates when compared with the image wavelet observed in the initial gradient. We analyze this phenomenon and demonstrate by example the effectiveness of the technique for subsalt targets.

Method

We consider the objective function arising from orthorhombic elastic propagations to be dependent on ten parameters: nine c_{ij} stiffness components and one density component r . We treat these 10 components as functions of 3 parameters, p-wave velocity V_p , s-wave velocity V_s , and ρ , while holding fixed the orthorhombic anisotropic parameters. We first formulate the 10-component gradients, and then project them into the 3-component form invoking the chain rule. We begin with the orthorhombic wave equation



$$\partial_t p = Ap + f, \quad (1)$$

where

$$p = \begin{bmatrix} V \\ \sigma \end{bmatrix}, A = \begin{pmatrix} 0 & bD \\ C(-D^*) & 0 \end{pmatrix}, f = \begin{bmatrix} f_V \\ f_\sigma \end{bmatrix}, V = \begin{bmatrix} V_1 \\ V_2 \\ V_2 \end{bmatrix}, b = \frac{1}{\rho},$$

$$\sigma = \begin{bmatrix} \sigma_{11} \\ \sigma_{22} \\ \sigma_{33} \\ \sigma_{23} \\ \sigma_{13} \\ \sigma_{12} \end{bmatrix}, C = \begin{pmatrix} c_{11} & c_{12} & c_{13} & \cdot & \cdot & \cdot \\ c_{12} & c_{22} & c_{23} & \cdot & \cdot & \cdot \\ c_{13} & c_{23} & c_{33} & \cdot & \cdot & \cdot \\ \cdot & \cdot & \cdot & c_{44} & \cdot & \cdot \\ \cdot & \cdot & \cdot & \cdot & c_{55} & \cdot \\ \cdot & \cdot & \cdot & \cdot & \cdot & c_{66} \end{pmatrix}, D = \begin{pmatrix} \partial_x & 0 & 0 & 0 & \partial_z & \partial_y \\ 0 & \partial_y & 0 & \partial_z & 0 & \partial_x \\ 0 & 0 & \partial_z & \partial_y & \partial_x & 0 \end{pmatrix}$$

Here p is the synthetic wavefield, V is the column vector of particle velocities, σ is the vectorized stress tensor notation according to Auld (1973), f_V and f_σ are the sources in particle velocity and pressure, respectively, b is the buoyance defined as $1/p$, and C is the abbreviated notation of the orthorhombic elastic stiffness matrix. The $*$ indicates the adjoint of an operator. Noticing $\partial x^* = -\partial x$, $-D^*$ is effectively obtained by taking D matrix-transposed. The FWI objective function $J = J(Sp, d)$, can be of any functional form that measures the data misfit. Here S is the sampling operator and d is the observed data. The differential of J in the set of parameters $m = [b, c_{11}, c_{22}, c_{33}, c_{13}, c_{12}, c_{44}, c_{55}, c_{66}]^T$, is

$$\frac{\partial J}{\partial m} = \frac{\partial J}{\partial (Sp)} \frac{\partial (Sp)}{\partial p} \frac{\partial p}{\partial m} \quad (2)$$

We distinguish the use of $\partial_m(\cdot)$ and ∇_m in that the former is a row vector when applied to scalar functions whereas the latter is a column vector being the transposed of the former. The "gradient vector" in m becomes

$$\nabla_m J = \left(\frac{\partial J}{\partial m} \right)^* = \left(\frac{\partial p}{\partial m} \right)^* S^* \nabla_{Sp} J \quad (3)$$

The data residual is

$$\nabla_{Sp} J = Sp - d \quad (4)$$

if we take $\|\cdot\|$ the L_2 norm and the objective function in a form $J = 1/2 \|Sp - d\|^2$. The gradient in p , V_p and V_s becomes

$$\begin{aligned} \nabla_p J &= \left\{ \frac{-V_p}{\rho^2} + v_p^2 [(1+2\varepsilon_2)\nabla_{c_{11}} + (1+2\varepsilon_1)\nabla_{c_{22}} + \nabla_{c_{33}}] + \frac{\partial c_{23}}{\partial \rho} \nabla_{c_{23}} + \frac{\partial c_{13}}{\partial \rho} \nabla_{c_{13}} + \frac{\partial c_{12}}{\partial \rho} \nabla_{c_{12}} + \right. \\ &\quad \left. v_s^2 \left[\frac{1+2\gamma_1}{1+2\gamma_2} \nabla_{c_{44}} + \nabla_{c_{55}} + (1+2\gamma_1) \nabla_{c_{66}} \right] \right\} J \\ \nabla_{v_p} J &= 2\rho v_p [(1+2\varepsilon_2)\nabla_{c_{11}} + (1+2\varepsilon_1)\nabla_{c_{22}} + \nabla_{c_{33}} + \frac{(1+2\delta_1)c_{33} - (1+\delta_1)c_{44}}{c_{23} + c_{44}} \nabla_{c_{23}} + \\ &\quad \frac{(1+2\delta_2)c_{33} - (1+\delta_2)c_{55}}{c_{13} + c_{55}} \nabla_{c_{13}} + \frac{(1+2\delta_3)c_{11} - (1+\delta_3)c_{66}}{c_{12} + c_{66}} \nabla_{c_{12}}] J \\ \nabla_{v_s} J &= 2\rho v_s \left[\frac{1+2\gamma_1}{1+2\gamma_2} \nabla_{c_{44}} + \nabla_{c_{55}} + (1+2\gamma_1) \nabla_{c_{66}} \right] J \end{aligned} \quad (5)$$



Here δ , ϵ and η are anisotropic Thomsen parameters described in Tsvankin (1997). We apply a simultaneous inversion to jointly update density, V_p and V_s .

Examples

We first show that by fitting the amplitude of reflections we produced relatively long length-scale velocity updates. We compare two cases: the two true models consist of a few layers on top, having values of 1.0km/sec, 2.0km/sec and 2.5km/sec in depth sequence, but one, shown in Fig. (1a), increases V_p to 3.5 km/sec in the half-space, whereas the other, shown in Fig. (1b), decreases V_p to 2.0km/sec. In both cases, we invert using full bandwidth of the data extending to 30hz, and start the inversion from the correct layered velocity on top extending 2.5km/sec to the rest of the model (Fig.1c). The outputs V_p (Fig.1d, 1e) show the correct step contrast in the bottom half-space, in which the long wavelength velocity update reaches a vertical scale much bigger than that of the image obtained using the maximum frequency of 30Hz of data. If we consider a local plane wave incident at the reflector (Fig. 1f) that has a scale of ΔL in the direction of propagation, the scale of the domain of influence along the reflector dip would be $\Delta Z_\theta = \Delta L / \cos(\theta)$, where θ is the secular opening angle. We conclude that the long scale update comes from wavelet stretch effect in the AVO residual at the large angles. Although the update due to wavelet stretched are weak relative to a short-offset image, the FWI iterations make it much stronger at the end of the optimization.

Our next example demonstrates a long length-scale update using the tomographic component within FWI. The true model, shown in Fig.2a, contains a shallow V_p anomaly with an 8% perturbation to the surrounding sediments. The deeper target has a velocity $V_p=2.7\text{km/sec}$. The starting model has the correct

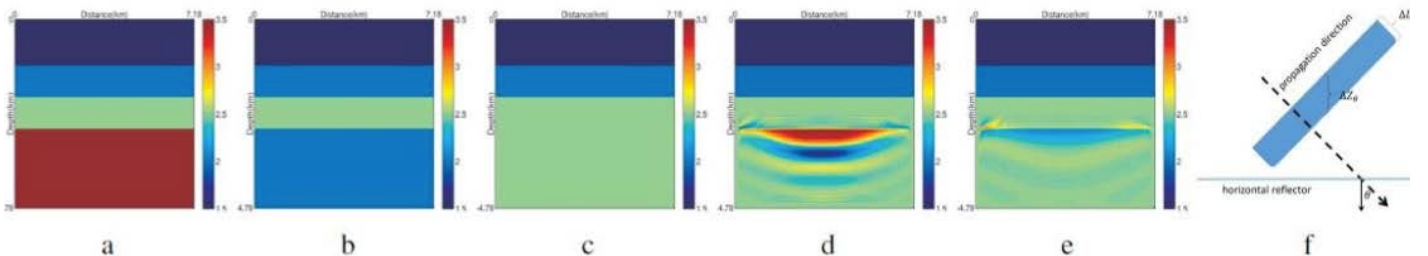


Figure 1. Wavelet stretch induced long length-scale update. (a) True velocity of the first case. (b) True velocity of the second case. (c) Initial velocity for both cases. (d) Output V_p for the first case. (e) Output V_p for the second case. (g) Schematic plot of a plane wave incident at an angle.

background (Fig.2b). The data is simulated with a maximum 30Hz Ricker wavelet and the diving waves are removed (Fig.2c). The initial gradient (Fig.2d) show the edges of the target but cannot fill in the body with correct velocity update. Forty iterations of L-BFGS produces the output V_p model shown in Fig. 2e. In this case, wavelet stretch effects fill in the anomaly from the top downwards, while the tomographic component, illustrated in Fig.2f, fills the anomaly from the base event upwards as the inversion proceeds. The anomaly is relatively small in magnitude, so shifts in the position of the base of the anomaly are relatively small as the anomaly is being filled in.

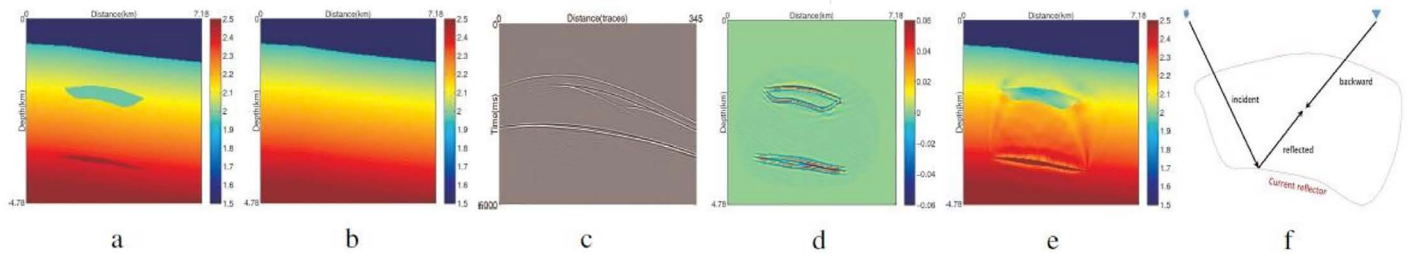


Figure 2. Tomographic long length-scale update. (a) True velocity. (b) Initial velocity. (c) Initial data residual. (d) Initial gradient. (e) Output V_p . (f) Schematic plot for tomographic update contained in FWI.

We show in the third example an orthorhombic inversion that combines the effects shown above from which the Vp and Vs for the garget subsalt reservoirs are recovered. We simulate the data with a Ricker wavelet peaked at 5Hz using elastic input models, Cij and , which come from a set of initial density model, a Vp model(Fig.3a) that has three 14% perturbed sub-salt anomalies, and a Vs model(Fig.3b) of 40% perturbations in the same region. The starting , Vp and Vs models hall have the correct background, including the salt, but are devoid of the sub-salt anomalies, shown in Fig.3c, 3d for Vp, Vs, respectively. The initial gradient in Vp and Vs via equation (5) contains clear crosstalks of p- and s- waves. Note both Vp and Vs gradients are of relative high frequency and neither of them has any in-fill of the target reservoirs. A 75

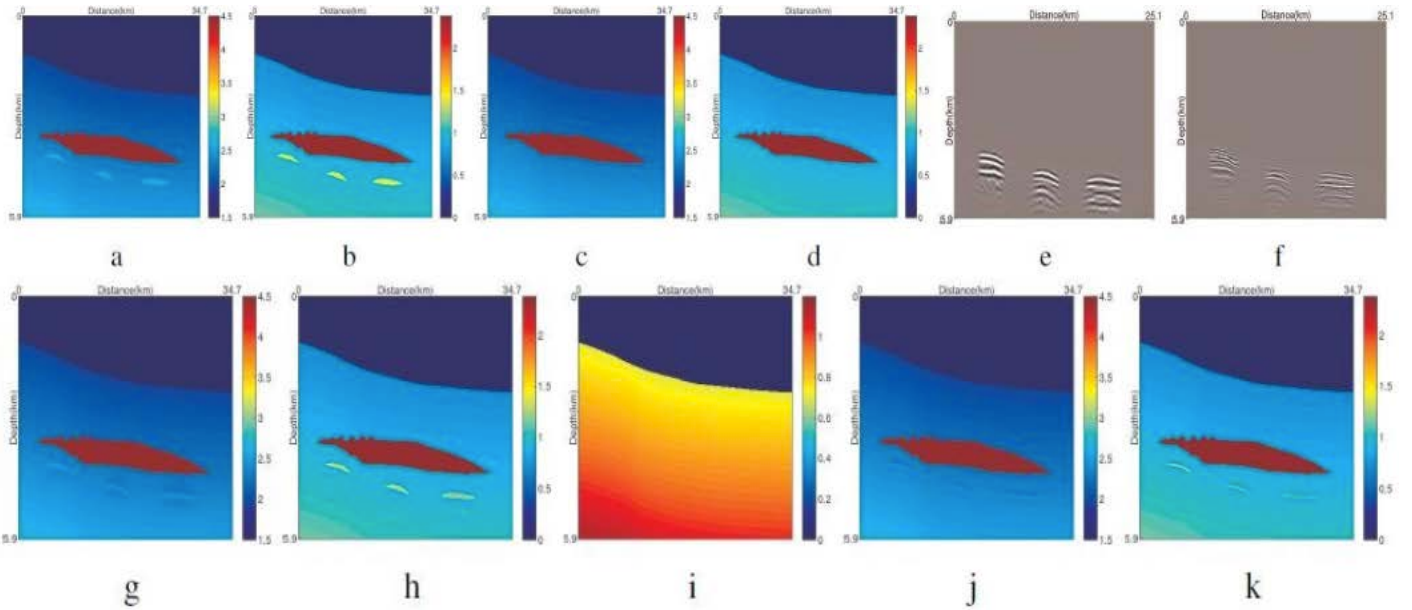


Figure 3. 2D and 3D orthorhombic FWI results. (a)True Vp model. (b) True Vs model. (c) Starting Vp model. (d) Starting Vs model. (e) Sub-salt gradient. (f) Sub-salt Vs gradient. 5. (g) Output 2D Vp model at iteration 75. (h) Output 2D Vs model at iteration 75. (i) Base perturbation for 3D anisotropy parameters. (j) Output 3D Vp model at iteration 25. (k) Output 3D Vs model at iteration 25.

We show as the last example an elastic inversion performed simultaneously for pressure wave velocity, shear wave velocity and density for a field data. Target areas were a shallow channel complex that was affecting amplitudes below and the reservoir channel complex below it. Shot gathers were relatively old vintage (2005) streamer acquisition. About 100 shots in two sail lines around two wells of interest were used for this inversion. Data was cropped to leave out very noisy large offsets and cables. A very light touch swell noise removal scheme was used in order to preserve AVO. Data was also filtered to a maximum frequency of 18 Hz. An initial wavelet was extracted from the water bottom and match filtered so that synthetics would better match the data. This process was done once at the beginning of the inversion only. Since synthetic wave propagation does not produce swell noise and other noise. The results are collected in Fig. 4. Comparing Fig. 4a, 4b, we see many details of pressure velocity are introduced. Likewise, the shear wave velocity has shown some improvements (Fig. 4c, 4d). Comparing to the initial density map (Fig. 4e), the density map (Fig. 4f) at the end of the 5th iteration correlates well with the Vp and Vs structures. The data matching is improving from the initial synthetic shown in Fig. 4g to the synthetic of the 5th iteration shown in Fig. 5h. The observed data is shown in Fig. 5i.

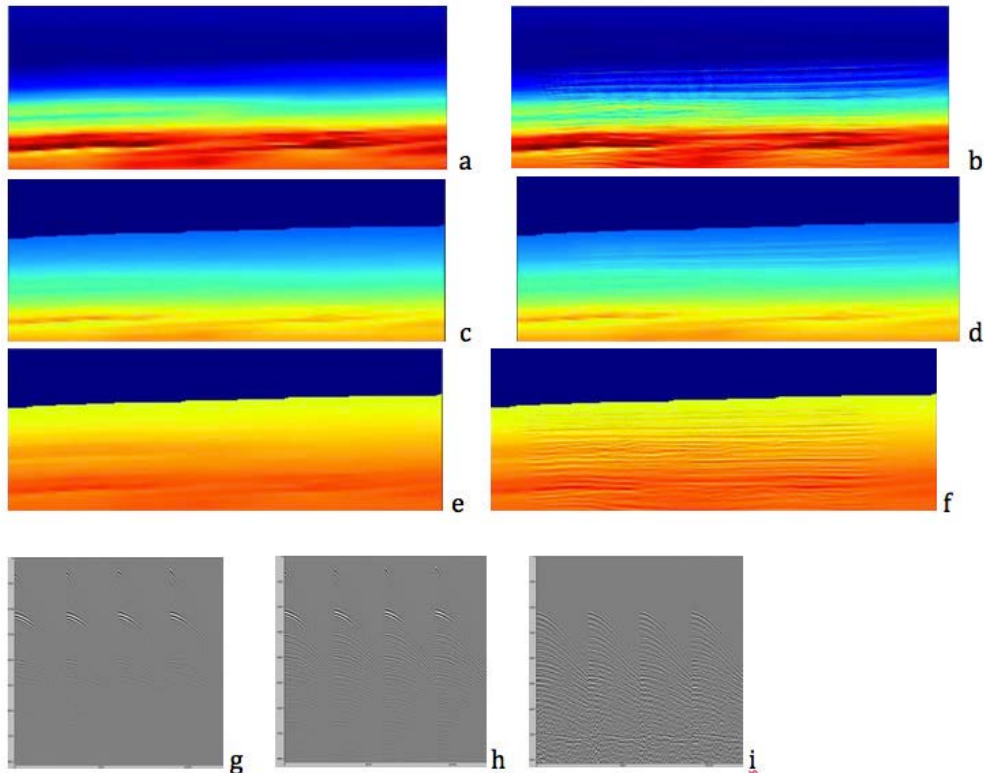


Figure 4 (a) Initial pressure velocity. (b) Inverted pressure velocity at iteration 5. (c) Initial shear velocity. (d) Inverted shear velocity at iteration 5. (e) Initial density model. (f) Inverted density at iteration 5. (g) Initial synthetic data. (h) Observed field data. (i) Synthetic data at iteration 5.

Conclusions

We have developed a constrained orthorhombic elastic multi-parameter FWI algorithm in the reflection domain and demonstrated its effectiveness in simultaneous inversion for pressure and shear velocity recovery associated with synthetic subsalt target sands. Cross talk between shear and acoustic models is significantly suppressed in the inversion process, while wavelet stretch and tomographic mechanisms recover long length-scale variations associated with the sands. Both 2D and 3D inversion recover the parameters effectively with values close to the true model values.

Acknowledges

We thank Lei Zhuo and Elizabeth Harvey for preparing the

sub-salt model. We thank Chevron Corporation for permission to publish this work.

References

- Albertin, U. 2015. Waveform inversion: Approaching a full bandwidth solution, presented at SEG Summer Research Workshop. FWI Applications from Imaging to Reservoir Characterization.
- Albertin, U., Shen, P., Anusha, S., Nihei, L., Johnsen, T., Wu, C. and Bub, K. 2016. 3D orthorhombic elastic full waveform inversion in the reflection domain from hydrophone data, Expanded Abstracts, Society of Exploration Geophysicists, 86th Annual International Meeting, 1094-1098. <https://doi.org/10.1190/segam2016-13866375.1>
- Auld, B. A. 1973. Acoustic Field and Waves in Solids. John Wiley & Sons, Inc.

Mora, P. 1988. Elastic wave-field inversion of reflection and transmission data. *Geophysics*, 53 (6), 750-759. <https://doi.org/10.1190/1.1442510>

Sears, T. J., Barton, P. J. and Singh, S. C. 2010. Elastic full waveform inversion of multicomponent ocean bottom cable seismic data: Application to Alba Field, U. K. North Sea. *Geophysics*, 75, 109-119. <https://doi.org/10.1190/1.1442510>

Tsvankin, I. 1997. Anisotropic parameters and P-wave velocity for orthorhombic media.

Geophysics, 1292-1309. <https://doi.org/10.1190/1.1444231>

Vigh, D., Jiao, K. and Watts, D. 2012. Elastic full-waveform inversion using 4C data acquisition.

Expanded Abstracts, Society of Exploration Geophysicists, 82nd Annual International Meeting. <https://doi.org/10.1190/1.1444231>

Author and Coauthor curriculum

Peng Shen Graduated from Rice University in 2004 with a Ph.D. degree in Computational and Engineering Science with a concentration in Geophysics. He had worked in seismic research unit for Total E&P and Shell International E&P. In 2014 he joined Chevron Corporation. His main focus since then has been elastic FWI. He is an active member of SEG and has about 30 journal or conference papers published since he joined the exploration industry.

Uwe Albertin received his doctorate in theoretical physics

from the University of California, Berkeley in 1989, and began his career in the seismic industry by joining the Research and Development Group of Western Geophysical in 1990. At Western, and later WesternGeco, he was initially involved with the technical development of velocity model and imaging algorithms, eventually becoming Team Leader and Geophysical Advisor for Depth Imaging. After fourteen years with WesternGeco, he joined BP as a Senior Research Geophysicist, serving as a project lead for imaging, velocity, and inversion algorithm development. After eight years with BP, he joined Chevron as a Geophysical Consultant, served as team lead for the Modeling and Inversion Research Group, and is currently project manager for waveform inversion, where he oversees the development of seismic wavefield modeling and inversion algorithms.

Anusha Sekar, originally from Chennai, India, Anusha Sekar received her Ph.D. in Mathematics at the University of Washington, Seattle. Her research interests at the UW included numerical analysis, numerical methods for wave propagation and geophysical inverse problems. She joined Chevron as in 2009 and has been working on various problems related to post-migration data conditioning with well data, amplitude vs. angle (AVA) techniques, seismic imaging and full waveform inversion (FWI). She is also the VP for the newly formed SIAM TX-LA section, working towards promoting collaboration between mathematicians in industry and academia in the Texas-Louisiana region.



Full Waveform Inversion for Resolving Complex Subsurface Velocities in Deepwater Gulf of México

Bin Yu (CGG), Ravi Kumar (CGG), Brad Wray (CGG), Katarina Jonke (CGG), Heiner Sarmient (CGG)

CMP2018_GC77

Artículo presentado
en el CMP / 2018

● Summary

Full Waveform Inversion (FWI) has been successfully applied to a wide range of datasets to resolve complex sediment velocities like gas clouds, shales, carbonates, etc. Most of the case studies using FWI focused on the improvements to overburden sediment sections and typically, an interpretive approach is taken for identifying the salt bodies. In the absence of clear images of sediment-salt interface, the interpretive approach relies on multiple scenarios to determine appropriate salt structure. Recently, BP demonstrated that from a good starting input model, long offset ocean bottom node (OBN) data could be used to effectively update some salt bodies such as salt fingers, overhangs salt shapes, dirty salt, mini basins and subsalt velocities to reveal better subsurface images. In this abstract, we demonstrate the application of FWI to a towed streamer datasets with limited offsets (<9 km) to successfully update salt and overhang velocity. For depth beyond the diving wave penetration, we used reflection FWI (RFWI) to further extend the reach of FWI and resolve the kinematic errors for deeper events. Our examples use a data driven velocity update flow from Perdido survey of Mexican waters of Gulf of México (GoM).

Introduction

Perdido fold belt of GoM is one of the prolific areas of world with blocks estimated to have significant hydrocarbon content. The water depths range from 1500 to 3500 m. The Perdido area is characterized by a compressional geology with large salt thrust sheets flowing over thick, highly folded sediment layers, resulting in many large anticlines - ideal setting for possible hydrocarbon accumulation. The folds hinder the advancement of the salt nappes, resulting in auto-sutures, rugose top of salt (TOS), imbricated sediment wedges and over turned carbonate and sediment sections. Other features of the region include thick bodies of mobile shale lying beneath folded sediments, overturned beds, and rafted carbonates on top

of the salt bodies. A typical vertical seismic section in Perdido fold belt area is displayed in figure 1. The supra-salt sediment velocities and the salt shape are critical for imaging reservoir targets that are typically present in the subsalt. In many regions, due to complex overburden, sediment velocities and salt shapes, targets cannot be accurately imaged by conventional top-down approaches that consist of angle/offset gather tomography coupled with top-down salt interpretation and salt scenarios.

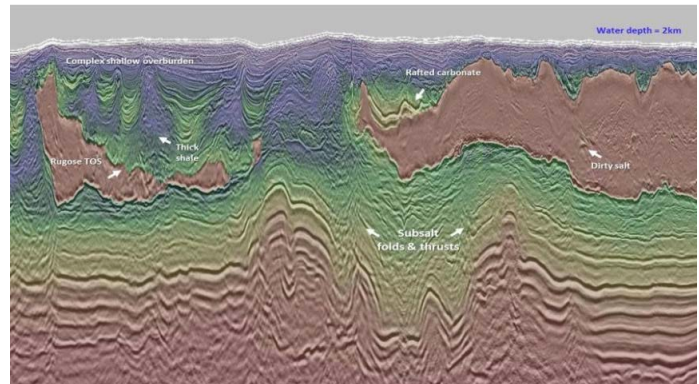


Figure 1 shows a typical section in Perdido area of GoM. The overburden velocities are very complex with many shale bodies, folded structures and carbonates above TOS. The subsalt structures are not completely resolved indicating velocity error from sediment and salt above.

Data driven approach for model building

Typical workflow for obtaining velocities comprises of a few iterations of ray tracing based tomography followed by a few iterations of salt interpretation and subsalt tomography using RTM based Surface Offset Gathers (SOGs). Although this flow gives a reasonable velocity model, it has severe shortcoming in the data misfit. All velocity updates are performed based on PSDM images such as common image gather (CIG) based event picking, stack image based salt interface interpretation, structural horizons based velocity retrending to name a few. An image

domain approach to the velocity model building tends to be limited by the amount of information available for velocity update. Since the velocity model is used to obtain the PSDM images, the gathers and/or stacks may be suboptimal as a result of destructive cancellation of primary events due to the large scale errors in the velocity model. Although several iterations can slowly improve the model, they are still far from resolving the complex part of the velocity model. Hence the complete information is not available for velocity update. This workflow fares well in regions with simple geology and velocities. However, in complex areas like Perdido, effectiveness of tomography is limited in the lateral and vertical resolution due to poor event picks.

On the other hand, we have the data domain approaches like FWI which hold the promise of providing detailed velocity models. It works by minimizing the least-square error between modeled and real seismic data (Tarantola, 1984). Its acoustic implementation is widely used and has shown promising results updating shallow overburden velocities over past years (Ratcliffe et al., 2011, Mothi et al., 2013, Zhu et al., 2014). Recently, Shen et al. (2017) successfully applied FWI with the OBN data having full azimuth coverage with offsets exceeding 20 km to update salt shape, overhang and subsalt velocities.

The major shortcoming of FWI is cycle skipping due to the lack of sufficient low frequencies. While the typical ray based workflows and salt scenarios approach may not resolve the detailed velocities, they are well suited for obtaining a good macro model. As long as the velocity errors in the macro model obtained is not too far from the true model, FWI can provide a meaningful velocity update. Hence, FWI is an ideal tool to resolve the overburden velocities and salt shapes with a starting model obtained from tomography and salt interpretation workflow. In this study, we use a WAZ data with smaller offset range and not as good low frequency signal compared to OBN survey. Yet, we were able to perform overhang and salt body update by FWI with the available WAZ data. With limited offset range, the FWI updates are limited by the maximum penetration depth of diving waves and we need other tools like RFWI to further update the deeper velocity.

With reflection information from deeper reflectors, RFWI is utilized to update the subsalt velocity after we exhaust the information provided by the diving energy. Nicholas and Gomes (2017) showed an RFWI flow that separates low wavenumber component from reflection FWI gradient to update velocity as outlined by Mora (1989). Density and velocity are updated from the high- and low-wavenumber components of the gradient respectively. The high-wavenumber update introduces

the sharp contrasts needed to generate back-scattered energy for the low-wavenumber velocity update. RFWI improves the match between synthetic and real data with updated velocities of relatively good lateral resolution (high k_x , k_y) and poor vertical resolution (low k_z).

Marine towed wide azimuth dataset

Our study uses a typical WAZ acquisition data (two streamer vessels and four source vessels) with maximum offset along the shooting direction of 8.1 km and maximum offset across the cable of 4.2 km. Our estimation showed that available offset range combined with the deep water environment resulted in diving wave-energy reaching at most about 4 km below the sea surface. We used data after noise attenuation for diving wave FWI which updates shallow overburden, overhang and salt bodies. Additional processing steps including source and receiver ghost removal, signature, and 3D surface-related multiple attenuation were applied to input to RFWI data for deeper section velocity update.

Overburden FWI for resolving sediments and overhang salt shapes

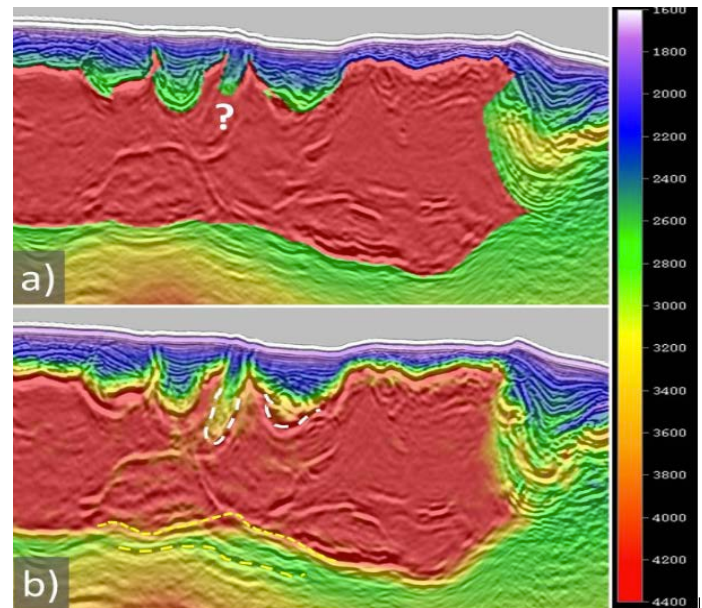


Figure 2 shows rugose salt body from Perdido section which containing thin salt fingers which are difficult for interpreters. Figure 2a shows the challenges that interpreters face and may disregard the thin basin (shown as "?") as part of salt while on the right carbonate sitting above TOS can be interpreted as salt because it has a strong impedance contrast with sediment. Figure 2b shows model and image after FWI update up to BOS. FWI successfully detected the sediment and salt boundary as indicated by the white dash line in figure 2b.

Figure 2 shows the motivation for our flow to update salt, overhang and sediment basins utilizing FWI. The rafted carbonates above top of salt (TOS) and the rugosity of TOS make it difficult to delineate the overburden velocity and salt sediment boundary with ray based tomography and manual interpretation. Carbonate sitting above TOS can have fast velocity close to salt velocity and result in strong impedance contrast with sediment above. Strong peak signal from top of carbonate can be mis-interpreted as TOS thus resulting in wrong salt body shape. On the right of figure 2a, there is a thick steep-dipping sediment basin with little to no hint of TOS which makes defining the salt flank subjective and leads to errors in the velocity model. Figure 2b shows the model and RTM image after FWI update including salt. It helps by clearly defining narrow sediment basin as well as correctly updating velocity for carbonate above TOS. For the steep TOS on the right, FWI detected the carbonate velocity and updated the sediment velocity between the carbonate and TOS. The improvement in image of TOS helps interpreters to better understand tectonics of salt movement and to improve BOS and subsalt image (yellow dash lines in figure 2b).

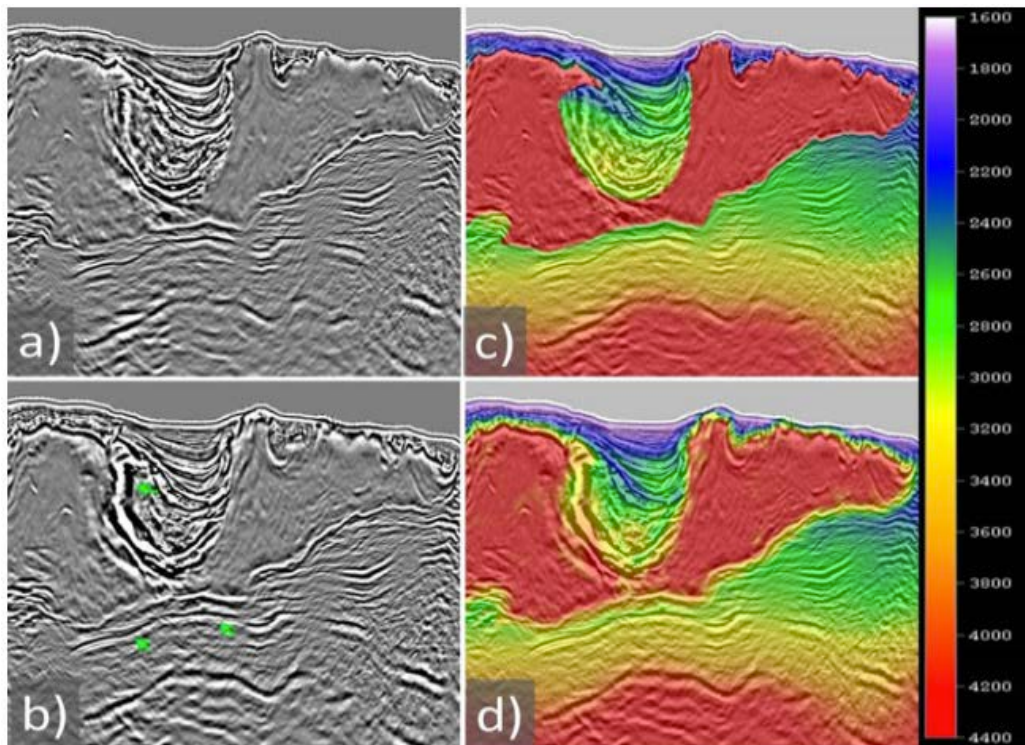


Figure 3 shows impact of updating salt and rafted carbonate encased inside an overhung basin. Figure 3a, c show RTM image and model based one conventional top down salt interpretation and velocity update. Figure 3b, d show improvement in image and model after salt and basin was updated with FWI respectively.

Figure 3 shows example from Perdido area with rugose salt shape. Initial salt interpretation was based on conventional top down method for velocity update. Salt interpretation looks reasonable based on image available. At many places TOS is not visible due to lack of impedance contrast between rafted carbonate sections and salt below the overhang basin. Not resolving the correct salt shape and velocity above base of salt (BOS) results in poor image in subsalt section. In figure 3a, the discontinuity at base of salt (BOS) indicates possible velocity errors above which are very hard to identify with conventional flow. We utilized diving wave FWI to update salt and carbonate above TOS. In figure 3d, FWI successfully updated the carbonate velocity resulting in better definition of the TOS and carbonate boundary. Imaging improvements were observed at BOS level and subsalt in figure 3b.

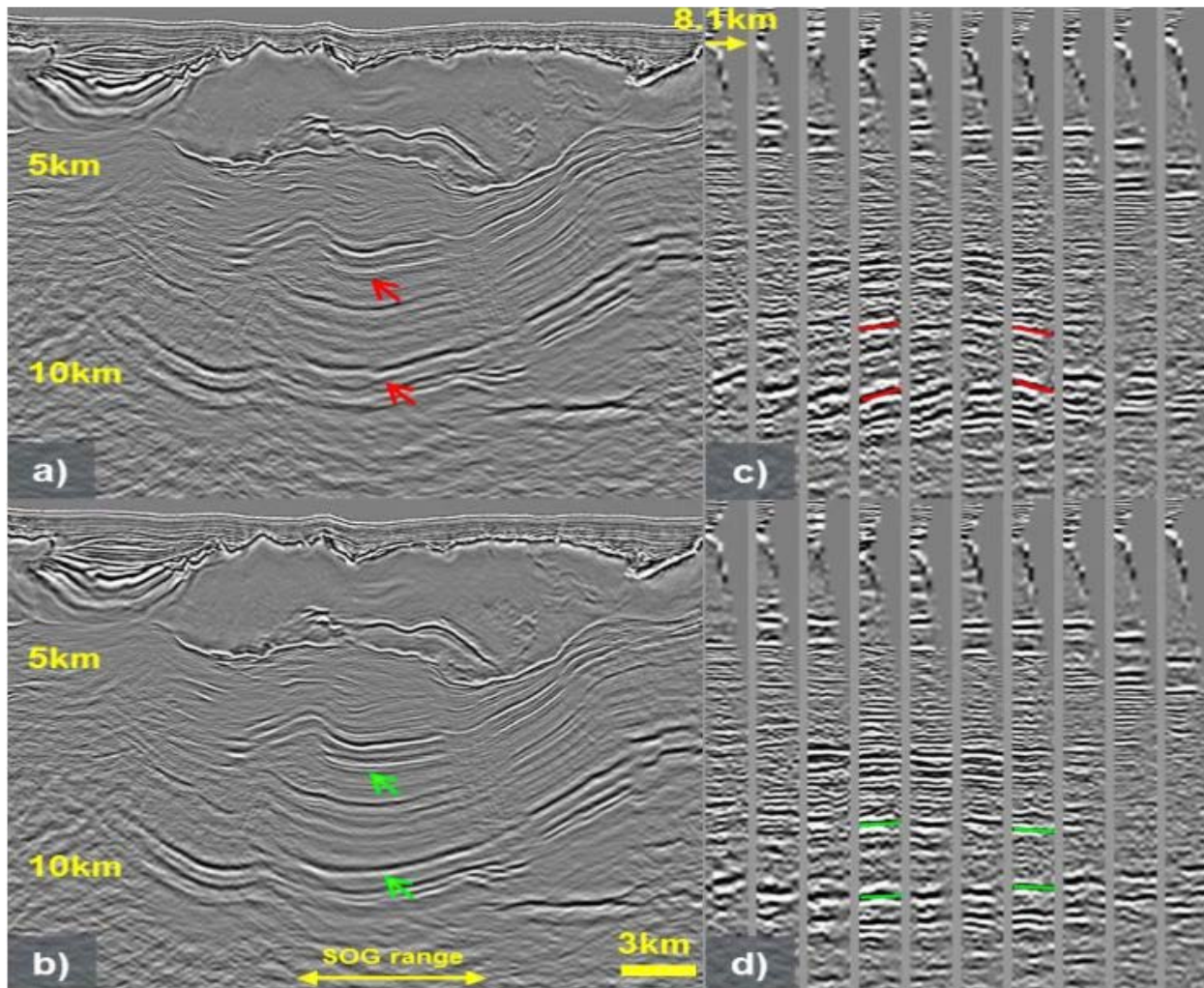


Figure 4 RTM stack from data migrated with a) initial model and b) RFWI updated model. RTM SOGs from data migrated with c) initial model and d) RFWI updated model.

Reflection FWI for subsalt update

Ray based tomography using RTM SOGs is a reliable tool for subsalt velocity update for certain geology settings. In Perdido fold belt area, there are many subsalt folds, thrusts, synclines and anticlines that can pose issues for curvatures based tomography. Figure 4c shows gathers with conflicting curvatures in the vicinity which requires tools with relative good lateral resolution to resolve. In such regions, ray based tomography lacks lateral resolution and it's too deep for diving wave based FWI to be effective. We used RFWI to update the subsalt velocity by reducing the kinematic errors using reflection energy. After RFWI, subsalt events are more continuous and SOGs are simpler and flatter (figure 4b, d). Undulations seen at Cretaceous layer introduced by velocity error above is mitigated by RFWI as indicated by arrows in figure 4a, b.

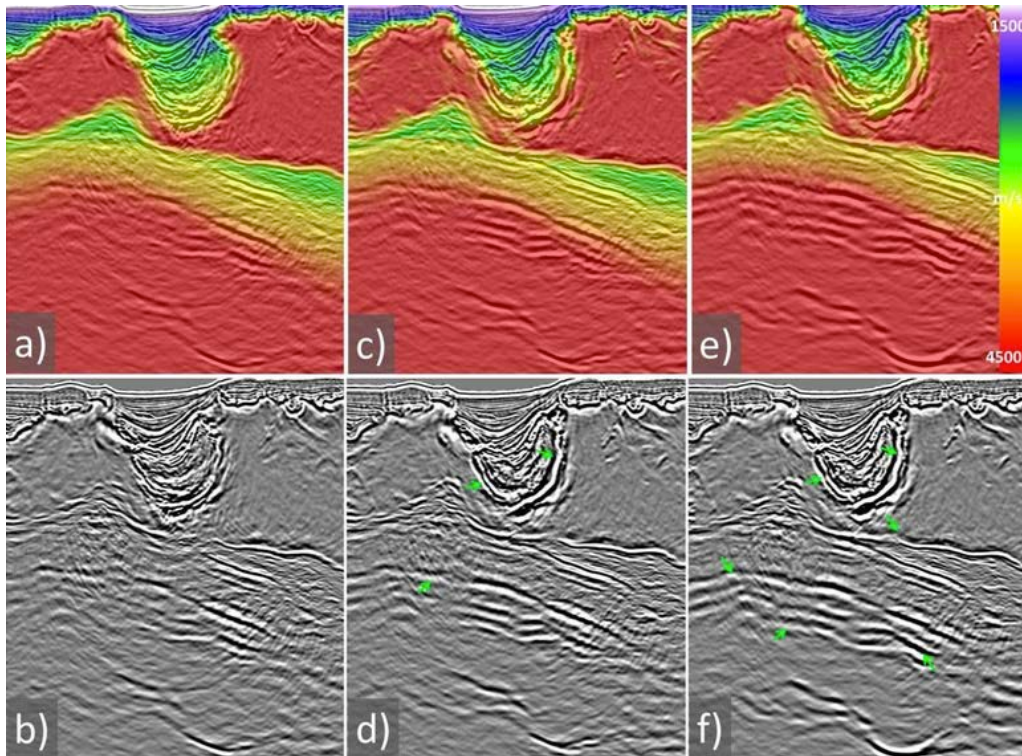


Figure 5 shows the velocity models at different stages of model update: a) initial model, c) FWI updated model, and e) FWI and RFWI model. The corresponding RTM stack are displayed in b) migrated with initial model, d) migrated with FWI updated model, and f) migrated with FWI and RFWI model.

Results

The combined impact of the FWI based data driven approach in figure 5. Figure 5a shows the velocity model after conventional tomography and salt interpretation which is the starting model for FWI and RFWI. Figure 5c shows the velocity model after diving wave FWI. The overhang and carbonate velocities are better defined after FWI (Figure 5c) which gives better BOS and subsalt image. At last, we applied RFWI to further update the subsalt velocity which improved the subsalt events coherency and simplified the structures (Figure 5e, f).

Conclusion and Discussion

In this study, we successfully applied diving wave FWI to update the shallow carbonate velocities and salt structures with towed streamer WAZ data. FWI detects carbonates and salt boundary effectively in the shallow which improves the BOS and subsalt image. For events beyond

the reach of diving wave energy, RFWI technique was employed. RFWI performs better over ray based tomography in subsalt folded structure, where we observed conflicting gather curvature in the same vicinity which is not an ideal situation for ray based tomography. RFWI extends our reach to update velocity in data domain by utilizing reflection energy. It resolved the overall kinematic error from shallow to the deep reflectors resulting in more imaged subsalt events and improving coherency. Although RFWI improves the subsalt image the major limitation is the lack of vertical resolution in the updated model.

The FWI and RFWI workflow extracts the kinematic information in recorded data to image the subsurface structure which helps to interpret the structure with more confidence. On the other hand, the conventional ray based tomography and interpretation driven approach could lead to image of "desired" structure due the bias in the interpretation used to derive the velocity model.

Acknowledgements

The authors would like to thank CGG Multi-Client & New Ventures and the Mexican Comisión Nacional de Hidrocarburos for permission to show these results.

References

- Chazalnoel, N., Gomes, A., Zhao, W. and Wray, B. [2017] Revealing shallow and deep complex geological features with FWI: Lessons learned. 79th EAGE Conference & Exhibition, Extended Abstracts, We A3 02.
- Gomes, A. and Chazalnoel, N. [2017] Extending the reach of FWI with reflection data: Potential and challenges. 87th SEG Annual International Meeting, Expanded Abstracts, 1454-1459.
- Irabor, K. and Warner, M. [2016] Reflection FWI. 86th SEG Annual International Meeting, Expanded Abstracts, 1136-1140.
- Liu, F., Zhang, G., Morton, S. and Leveille, J. [2011] An effective imaging condition for reverse-time migration using wavefield decomposition. *Geophysics*, 76(1), S29-S39.
- Mothi, S., Schwarz, K., and Zhu, H., [2013] Impact of Full-azimuth and Long-offset Acquisition on Full Waveform Inversion in Deep Water Gulf of Mexico. *SEG Technical Program Expanded Abstracts 2013*: pp. 924-928.
- Mora, P. [1989] Inversion = migration + tomography. *Geophysics*, 54(12), 1575-1586.
- Ratcliffe, A., Win, C., Vinje, V., Conroy, G., Warner, M., Umpleby, A., Stekl, I., Nangoo, T., and Bertrand, A. (2011) Full waveform inversion: A North Sea OBC case study. *SEG Technical Program Expanded Abstracts 2011*: pp. 2384-2388.
- Shen, X., I. Ahmed, A. Brenders, J. Dellinger, J. Etgen and S. Michell, 2018, Full-waveform inversion: the next leap forward in subsalt imaging. *The Leading Edge*, 67b1-67b6
- Sun, D., Jiao, K., Cheng, X. and Vigh, D. [2016] Reflection based waveform inversion. 86th SEG Annual International Meeting, Expanded Abstracts, 1151-1156.
- Tang, Y., Lee, S., Baumstein, A. and Hinkley, D. [2013] Tomography enhanced full wavefield inversion. 83rd SEG Annual International Meeting, Expanded Abstracts, 1037-1041.
- Tarantola, A. [1984] Inversion of seismic reflection data in the acoustic approximation. *Geophysics*, 49(8), 1259-1266.
- Zhu, Huifeng & Chazalnoel, N & Zhao, W. (2014). Building a High-resolution Model with Full Waveform Inversion in Deep Water West Africa. *10.3997/2214-4609.20141416*.

Professional career of the author and co-authors

Bin Yu. Ph.D. in Space Physics from Rice University with 10 years of experience. He currently holds the position of Imaging Team Leader at CGG.

Ravi Kumar. M.S. in Geological and Earth Sciences from Rice University With 10 years of experience. He currently holds the position of Senior Imaging Project Leader at CGG.

Brad Wray. Ph.D. in Physics from University of Texas at Austin with 7 years of experience. He currently holds the position of Imaging Team Leader at CGG.

Katarina Jonke. M.S. in Geophysics from University of Houston. She currently holds the position of Imaging Team Leader at CGG.

Heiner Sarmiento. M.Sc. in Physics from Industrial University of Santander - UIS, with 8 years of experience. He currently holds Senior Imaging Project Leader position at CGG.



Boletín Técnico AMGE

Segunda Generación



Asociación Mexicana de Geofísicos
de Exploración, A.C.

Para someter manuscritos en el Boletín Técnico AMGE
–Segunda Generación, así como conocer las normas editoriales
y guía de publicación, favor de comunicarse con alguno
de los siguientes editores:



Raúl del Valle García
Email: rvalleg@imp.mx



Efraín Méndez Hernández
Email: emendez2310@gmail.com





Congreso Mexicano del Petróleo

León, June 19th-22th, 2019



Mexican Petroleum Conference 2019

The Mexican Association of Exploration Geophysicists (AMGE) is pleased to invite you all to The Mexican Petroleum Conference and Exhibition León 2019, organized and operated as a joint venture of the five professional associations which conglomerates most of the technical specialties of the O&G Mexican Industry namely: Association of Petroleum Engineers of México (AIPM), Society of Petroleum Engineers, (SPE México Section), Petroleum Engineers Mexican College (CIPM), Mexican Association of Petroleum Geologists (AMGP) and also AMGE as this year organization leader.

Mexican Petroleum Conference (CMP) year by year brings together more than 8,000 attendees including: Industry leaders, renowned National and International Technical Specialists, Experienced and Young professionals as well as college and master degree students coming from up to 30 different countries. Presently, considered the biggest and most important event O&G Conference in Latin America, it is the ideal forum to display the most remarkable achievements and technical advances, specially in E&P but covering and strengthening transforming and transporting as years has passed.

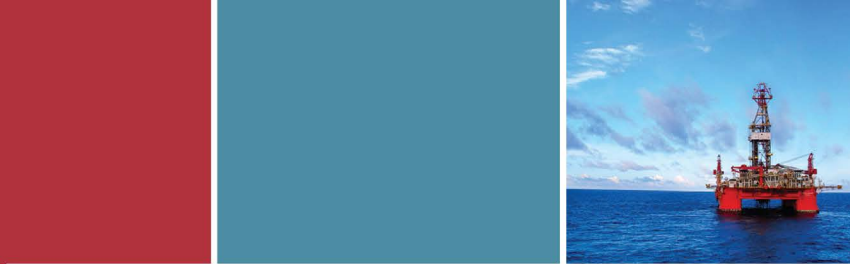
This year, the technical program for this 14th edition includes pre-conference short courses and workshops, 150 oral presentations and 90 e-poster sessions, besides some Luncheon Conferences, Technical Forums, remarkable master and distinguished lectures.



Exhibition

18,000sqm of industrial exhibition will gather together a well selected sample of the most important O&G National and International products and services Companies and operators. With an expected presence of about 190 different brands and firms the CMP Exhibition will be the perfect sized complement of the technical program, occupying some number around 1,000 booths.

All this ingredients will make León CMP 2019 the perfect spot to look for technical and business opportunities which might be there at your fingertips!



Who are expected to be there?

- O&G Operators
- O&G Industry leaders
- O&G Decision makers
- Engineers
- Head Hunters
- Products and Equipment Suppliers
- Service Companies
- Business developers
- Specialized media



General Program

- ➔ Magistral Conferences
- ➔ Panel Discussions
- ➔ 150 Technical Sessions
- ➔ 90 e-poster sessions
- ➔ Luncheon Conferences

León, Guanajuato

México is ranked as the second largest economy in Latin America and the fourteenth largest in the world. This, combined with its abundance of natural attractions, cultural offerings, specialized infrastructure and its range of first class leisure activities, has resulted in the rapid growth of the Meetings Industry (Meetings, Incentives, Congresses and Exhibitions).

León, the capital of the state of Guanajuato, is the ideal destination to enjoy springs, hot springs and buy the most high quality shoes in México.

Poliforum León offers all kind of facilities and confort of a first level Convention Center to ensure every event success. It accounts with 45,000sqm of building, including 23,000sqm of exhibition floor clear of columns in just one single level, which results ideal to display all kind of exhibitions.



